A Mapping Survey of the ^{13}CO and ^{12}CO Emission in Galaxies

Timothy A. D. Paglione[1,2,3], W. F. Wall[4], Judith S. Young[1,2], Mark H. Heyer[1,2], Michael Richard[2], Michael Goldstein[2], Zeke Kaufman[2], Julie Nantais[2], Gretchen Perry[2]

paglione@umich.edu

ABSTRACT

We present spectra of the extended ^{12}CO and ^{13}CO $J=1\rightarrow 0$ emission along the major axes of 17 nearby galaxies. Spatial variations in the ratio of CO and ^{13}CO integrated intensities, $\mathcal{R}$, are found in nearly every galaxy observed. There is an overall variation in $\mathcal{R}$ of 20–40% from the inner 2 kpc to the disk. Roughly a third of the survey galaxies have such gradients in $\mathcal{R}$ detected above the 2σ confidence level. Though some galaxies show a lower central value of $\mathcal{R}$, on average $\mathcal{R}$ inside 2 kpc is 10–30% higher than $\mathcal{R}$ outside of 2 kpc. The average CO/^{13}CO intensity ratio within the central 2 kpc of the survey sources is 11.6 ± 0.4 (based on the noise) ±1.5 (based on systematic uncertainties estimated from daily variations in CO and ^{13}CO intensities). The 1σ dispersion in $\mathcal{R}$ between galactic nuclei of 4.2 is also quite large. The average value of $\mathcal{R}$ outside 2 kpc is $9.8\pm0.6\pm1.2$ with a standard deviation of 4.5.

An increase in the CO/^{13}CO intensity ratio from disk to nucleus may imply that the conversion factor between CO intensity and H_2 column density, X, is lower in galactic nuclei. Also variations in physical conditions, most notably the gas kinetic temperature, affect both $\mathcal{R}$ and X. Abundance variations probably do not cause the gradient in $\mathcal{R}$, though we do not rule out a decrease in effective cloud column densities in galactic nuclei possibly caused by destructive starburst superwinds. A modest rise in temperature (less than a factor of 2 or 3) from outside a 2 kpc radius towards the nucleus can easily account for the observed

[1]Five College Radio Astronomy Observatory

[2]Department of Astronomy, Lederle Graduate Research Center, University of Massachusetts, Amherst, MA 01003

[3]Current address: Department of Astronomy, University of Michigan, 500 Church St., Ann Arbor, MI 48109-1090

[4]Instituto Nacional de Astrofísica, Optica y Electrónica, Apartado Postal 216 y 51, 72000 Puebla, Pue., México

gradient. These results support previous work implying that X is lower in the center of the Milky Way and probably most galactic nuclei. Therefore calculating H_2 masses using the standard Galactic X-factor, especially within the central few kpc of galaxies, overestimates the true mass by factors of a few. The standard X-factor still appears to be appropriate for galactic disks.

Subject headings: galaxies: ISM, starburst — ISM: clouds, molecules

1. Introduction

Central to a complete picture of galaxy evolution is understanding star formation over large scales. Given that stars form in molecular gas, the evolution of a galaxy depends on its gas distribution. The main constituent of this gas is molecular hydrogen, which, due to its symmetry, has no dipole transitions between low-lying levels (i.e., no permitted rotational transitions). Consequently, the rotational lines of carbon monoxide and its isotopic variants (e.g., ^{13}CO and C^{18}O) have been used to study molecular gas in galaxies. The millimeter-wave lines of CO are the brightest among non-masing molecular transitions. In particular, the $J=1\rightarrow 0$ line of ^{12}CO (hereafter written simply as CO) has been invaluable for determining the distribution of molecular gas column densities within the Milky Way and other galaxies (Dame, Hartmann & Thaddeus 2001; Young et al. 1995).

These distributions are inferred assuming that the molecular gas column density, N_{H_2}, is traced by the velocity-integrated radiation temperature (Rayleigh-Jeans brightness temperature), $I(\mathrm{CO}\,J=1\rightarrow 0) \equiv \int T_R dv$. Though the CO emission is usually optically thick and consequently may not reliably trace column densities, the ratio N_{H_2}/I_{CO}, or "X-factor," is found to be roughly constant on the size scales of many parsecs, with a value of $X = 1.6\times 10^{20}\,\mathrm{cm}^{-2}\,(\mathrm{K\ km\,s^{-1}})^{-1}$ in the Galactic disk (Dame, Hartmann & Thaddeus 2001; Hunter et al. 1997). The conventional explanation of how the optically thick CO line consistently measures column density requires that giant molecular clouds are in self-gravitational equilibrium and that the mean density and temperature do not significantly vary from cloud to cloud (Dickman, Snell & Schloerb 1986; Sakamoto 1996). Despite these results, there is evidence that X is 2–10 times lower than the standard value in the central few hundred parsecs of the Galaxy (Sodroski et al. 1995; Dahmen et al. 1998). It may also increase by 2–4 times the standard value in the outer Galaxy (Digel et al. 1990; Sodroski 1991; cf., Carpenter et al. 1990). Nonetheless, a secondary measure of gas column density is required to gauge any variation of X with galactocentric radius.

There are suggestions in the literature both for and against the X-factor varying with

position in external galaxies, often from observations of the rotational lines of ^{13}CO, a rarer isotopic variant of the more commonly observed CO. Since ^{13}CO is 30–70 times less abundant than CO (e.g., Langer & Penzias 1990), its rotational lines are usually optically thin on parsec scales. Therefore, assuming similar molecular gas physical conditions, observations of ^{13}CO can give reliable molecular gas column densities, and any variation in the ratio of CO and ^{13}CO $J=1\rightarrow 0$ integrated intensities, $\mathcal{R}$, can then test whether X varies systematically within galaxies. Rickard & Blitz (1985) claim that this ratio is up to a factor of 5 higher in the central $1'$ than in the disks of six galaxies, implying that X is up to 5 times smaller in galaxy centers. In contrast, the CO/^{13}CO intensity ratios observed by Young & Sanders (1986) and Sage & Isbell (1991) show no significant differences between the centers of spiral galaxies and their disks. However, any study of molecular gas column densities that uses ^{13}CO lines must address the uncertainty in assumptions such as the ^{13}CO abundance, the gas kinetic temperature, and whether local thermodynamic equilibrium (LTE) applies. Also, $\mathcal{R}$ is a sensitive function of optical depth. Hence, any observed variation, such as found by Rickard & Blitz (1985), could be attributed to variations in the ^{13}CO abundance or excitation, rather than a spatial variation in X. Though separating these variations from other effects requires observations of other lines (e.g., ^{13}CO $J=3\rightarrow 2$) and isotopic variants (e.g., C^{18}O), a gradient in $\mathcal{R}$ would indicate an important variation in the physical or chemical properties of the molecular medium of a galaxy.

In this paper, we present the results of a survey of the $J = 1 \rightarrow 0$ lines of ^{13}CO and CO along the major axes of 17 galaxies (see Table 1). Unlike previous surveys, systematic uncertainties between intensities at different positions are reduced by using a receiver array. The array also permits efficient fully-sampled mapping of many positions in a galaxy.

2. Observations and Data Reduction

The data were obtained between 1998 December and 2000 May at the Five College Radio Astronomy Observatory (FCRAO) 14 m telescope. We observed the CO and ^{13}CO $J=1\rightarrow 0$ lines (115.27 and 110.20 GHz) with the MMIC-based, 4×4-element array, SEQUOIA (Erickson et al. 1999). The beam FWHM at 115 GHz was $45''$, and the main beam efficiency was ~ 0.5. The pixel spacing on the sky was $1\rlap{.}'476$, or roughly two full beam widths. System temperatures were 130–400 K at 110 GHz, and 200–1200 K at 115 GHz. We used the facility broad-band filterbank, comprised of 64 channels of 5 MHz width, which yielded a velocity resolution of 13 $\mathrm{km\,s^{-1}}$ at 115 GHz.

The observed galaxies are the brightest and most extended from the FCRAO Extragalactic CO Survey of Young et al. (1995) that are primarily within the R.A. range of

9–16 hours (Table 1). The array was aligned with the major axis of each galaxy, and moved from the edge of the CO disk across its full extent, with measurements taken at half-pixel (roughly half-beam) spacing. Thus each map position was observed with all four receivers of a row. Fully sampled maps were not made along the minor axes. Rather, off-axis data were obtained from the rows of the array parallel to the major axis, offset by $\pm1'\!.476$ and $\pm2'\!.952$.

Except for NGC 253, which has a low declination, we observed above an elevation of 30° to avoid large gain variations. We also observed below an elevation of 75° to avoid any possible tracking errors. The pointing and focus were checked regularly on SiO maser sources and Jupiter, and calibration was done every several minutes using the chopper wheel method. A linear baseline was removed from all spectra. Those requiring higher order fits were discarded. Spectra with r.m.s. noise levels significantly different from those expected given the system temperature were also discarded. These data typically resulted from poor calibrations or non-linear baselines caused by quickly varying conditions. The filtered data were then coadded, weighted by the noise ($1/\sigma^2$). Therefore the largest calibration offsets, caused by low elevation and poor weather, contributed less to the overall results. Relative gain variations between pixels were well below 10%, and since each map position was observed by all four pixels in a row, this uncertainty was further reduced.

To assess systematic uncertainties, the line integrated intensities were monitored for day-to-day variations (mostly at the central position). The weighted average CO and ^{13}CO intensities on any given day varied from the total season's weighted average by 5–25% and 15–50%, respectively. Any data with obvious offsets in pointing (evident as markedly different spectral line shapes), or calibration (anomalous line and noise temperatures) were discarded. In sum, the *relative spatial variations* in the CO and ^{13}CO intensities, and their ratio, are very well determined for each galaxy. However, the systematic uncertainties in $\mathcal{R}$, which are important for comparing the intensity ratios between galaxies, are roughly 15–60% (Table 2). Most of these systematic variations are likely due to slight pointing offsets along the minor axis, which are difficult to detect in low signal-to-noise spectra, and do not strongly affect the line shapes. Periodic observations of Jupiter indicate that the uncertainties due to variations in calibration contribute no more than 15–20% to the systematic uncertainty in line intensity.

3. Results

Emission from both CO and ^{13}CO is detected at nearly every mapped position along the major axes of these galaxies. Off-axis emission $> 1'\!.5$ away from the major axis, is detected only in the less inclined galaxies IC 342, M51 and NGC 6946. Due to the low signal-to-noise ratio of the ^{13}CO spectra off-axis, we do not include those data in the analysis. Figure 1

shows the spectra along the major axes of the survey galaxies. The similarity of the CO and ^{13}CO line shapes with position demonstrates the good relative pointing (better than 5″) between the observations. The line integrated intensities ($\int T_A^* dv$) and CO/^{13}CO intensity ratios ($\mathcal{R}$) as functions of position along the major axis are shown in Figure 2.

The unweighted average of the CO/^{13}CO intensity ratio in the beam centered on the nucleus is $11.5 \pm 0.3 \pm 1.4$, given the statistical and systematic uncertainties, respectively (Table 2). Statistical uncertainties are based on the r.m.s. noise, line width and channel width, and systematic uncertainties are estimated as described at the end of § 2. The standard deviation in $\mathcal{R}$ from one galaxy center to another is 5.4. The weighted average central ratios are 9.0 ± 0.2 and 7.7 ± 0.6 based on the statistical and systematic uncertainties, respectively. The central ratios for M51 and M82 deviate significantly from these values. The high ratio of 27 ± 8 for M82 is consistent with previous studies (e.g., Stark & Carlson 1982; Young & Scoville 1982; Loiseau et al. 1988; Kikumoto et al. 1998). However, the low ratio of 5.4 ± 1.0 for M51 is nearly a factor of 2 below some previous observations (Young & Sanders 1986; Garcia-Burillo et al. 1993). The individual CO and ^{13}CO data for M51 were taken over several widely separated days, and cover a large range in elevation, weather conditions, and times of day. Despite the varied conditions, the data sets agree well with one another (the estimated systematic uncertainties are 13 and 14% for CO and ^{13}CO, respectively, yielding a 19% uncertainty in $\mathcal{R}$). The relative pointing was consistent, judging by the line shapes and radial intensity profiles. Therefore, we do not correct our values for M51 for any possible calibration offset, though we will draw no strong conclusions from the low ratio. We point out that our observing technique still results in a very low relative uncertainty in the spatial variation in $\mathcal{R}$ within the disk of M51.

Figure 2 indicates that nearly all the galaxies show some significant variation in $\mathcal{R}$ with position. The most prevalent trend is for $\mathcal{R}$ to drop with galactocentric distance. The gradient in $\mathcal{R}$ is more apparent and significant after the line intensities are binned to make the uncertainty in $\mathcal{R}$ more uniform (Figure 3). Here non-detections have been excluded. The calculated uncertainties in these average ratios are multiplied by $\sqrt{2}$ to account for the interdependence of the Nyquist sampled data. This correction is conservative and may overestimate the error by about 20% for small bin sizes. Table 2 and Figure 4 compare the weighted average values of $\mathcal{R}$ inside and outside of various radii. Figure 4 shows that for many galaxies, $\mathcal{R}$ drops by as much as a factor of 2 between the central and outer disk. On average, $\mathcal{R}$ within a radius of 2 kpc is 40% higher than the disk value. No correlations are found between distance and $\mathcal{R}$ nor its gradient (Figure 4).

Several galaxies show a significant change in the gradient in $\mathcal{R}$ with the size of the central bin (Figure 5). Note that typically the change in $\mathcal{R}$ does not depend strongly on the

central bin size, so the adopted distance to a galaxy is not very important. For those with significant changes, the bin size simply scales with distance, and intermediate values of $\mathcal{R}$ still lie on the trends shown. For NGC 253 and NGC 2146, the disk ratio decreases with the size of the central bin. The CO intensity distribution in NGC 253 is strongly centrally peaked inside 2 kpc. For NGC 2146, several outer points are not detected in ^{13}CO, so its distribution in the disk appears flatter than it may be (Figure 2), and the change in $\mathcal{R}$ is somewhat biased by this sensitivity limit. For NGC 3556, NGC 4631 and NGC 6946, the central ratio decreases with the size of the central bin, and the gradient in $\mathcal{R}$ also decreases. NGC 3556 and NGC 4631 have flatter CO and ^{13}CO distributions with peaks offset from the center by 1.5–2 kpc that are more pronounced in ^{13}CO emission. The CO distribution for NGC 6946 peaks more sharply than the ^{13}CO at the nucleus. The central ratio increases with bin size for IC 342, NGC 3593 and NGC 3627. Their ^{13}CO distributions are more strongly centrally peaked within 1 kpc than the CO. M82 is unusual in that $\mathcal{R}$ in the disk increases as the central bin increases from 0.7 to 1.5 kpc radius, but then decreases for a central bin of 2 kpc radius.

4. Discussion

4.1. Possible Causes of Variations in the CO/^{13}CO Intensity Ratio

Various physical mechanisms could cause a gradient in the observed CO/^{13}CO intensity ratio. The most obvious are changes in the relative CO and ^{13}CO abundances, and beam-averaged optical depths. A gradient in the X-factor, which may depend on the gas density and/or temperature, could also be responsible. For the following discussion, we assume, based on the centrally peaked profiles of integrated intensity (Figure 2), that the total beam-averaged H_2 column density increases towards the nucleus of each survey galaxy. Also, we assume that $\mathcal{R}$ generally decreases with galactocentric distance. (It increases with radius only for NGC 3628, NGC 5055 and M51, and their individual ratios at large radii are still low.)

4.1.1. Abundances

There is a clear positive gradient in the ^{12}C/^{13}C abundance ratio in the Milky Way (e.g., Langer & Penzias 1990, and references therein). It rises linearly from a value near 30 within 4 kpc of the Galactic center, to ~ 70 at 10 kpc, and is most likely due to stellar processing of matter during the lifetime of the Galaxy; older populations have enhanced the ^{13}C in the

bulge. However, this gradient is in the opposite sense of the gradient in $\mathcal{R}$ seen here and in the Milky Way. For example, large-scale maps of the Milky Way suggest that $\mathcal{R}$ varies from 10 ± 3 in the central 2 kpc to 6 ± 1 from 2 to 8.5 kpc (A. Luna, private communication), which is very similar to the results of this survey. Though $\mathcal{R}$ appears to be roughly constant at ~ 5 throughout most of the Galaxy (e.g., Solomon, Sanders & Scoville 1979; Polk et al. 1988; Oka et al. 1998), large-scale observations may yield higher values of $\mathcal{R}$ due to the inclusion of CO emission from very diffuse gas not detectable in ^{13}CO emission (Polk et al. 1988; Lee, Snell & Dickman 1990). Also, the generally low CO/^{13}CO intensity ratios seen in galaxies indicate that at least the CO emission is optically thick, and therefore $\mathcal{R}$ is a poor tracer of the ^{12}C/^{13}C abundance ratio.

Another argument against stellar processing affecting $\mathcal{R}$ is that a correlation should exist between $\mathcal{R}$ and the C^{18}O/C^{17}O intensity ratio assuming that the stellar populations in the starburst nuclei of these galaxies contain relatively few low to intermediate mass stars (those responsible for much of the ^{13}CO generation) (Sage, Henkel & Mauersberger 1991). However, such a correlation is not observed. In particular, the C^{18}O/C^{17}O intensity ratio for M82 of ~ 8 is similar to that of NGC 253 and IC 342, whereas the central CO/^{13}CO intensity ratio of M82 is twice those of the other galaxies. Casoli, Dupraz, & Combes (1992) also suggest that the CO abundance could increase by a factor of two due to an enhanced production of CO by massive stars. However, given the high optical depth of CO, this change will not alter $\mathcal{R}$. Further, Taniguchi et al. (1999) attribute the high ratios seen in some galactic nuclei to a *deficit* of ^{13}CO, not an enhancement of CO.

It has been suggested that the CO isotopic abundances may be altered by mechanical means as well. The high central CO/^{13}CO intensity ratios (> 20) seen in the nuclei of some mergers and ultraluminous starburst galaxies (Casoli et al. 1992a; Aalto et al. 1991; Henkel & Mauersberger 1993; Taniguchi et al. 1999), are thought to be due to either transport of less-processed (^{13}CO-poor) disk gas to the nucleus via an interaction, or destruction of dense (^{13}CO-rich) clouds by nuclear superwinds. If gas transport occurs faster than ^{13}CO production in the nucleus, any gradient should be erased. Models of galactic bars show that abundance gradients are indeed flattened after roughly 10^9 yr (Friedli, Benz & Kennicutt 1994), and that mass inflow time scales for slightly perturbed spirals are $\lesssim 10^9$ yr, and shorter for stronger interactions (Jog & Das 1992, and references therein). That the gradient in $\mathcal{R}$ for the Milky Way opposes the ^{12}C/^{13}C abundance gradient also implies that altering abundances seems to have little effect on the CO and ^{13}CO emission. Further, NGC 3628 and M51 are two of the few galaxies in this survey with positive gradients in $\mathcal{R}$, yet they are clearly in interactions. Therefore, unless a merger injects ^{13}CO-poor gas directly into a nucleus, transport due to bars or interactions seems unlikely to produce this gradient. The observed gradient in $\mathcal{R}$ instead favors the superwind argument since $\mathcal{R}$ and the star formation rate in

these galaxies are generally higher in the nucleus than in the disk. However, the volume and column densities of the gas toward these galactic nuclei are typically inferred to be large (e.g., Paglione, Jackson, & Ishizuki 1997). Therefore, if a superwind causes the higher CO/^{13}CO intensity ratio in the nucleus, it must force the clouds into many very small, dense clumps. This possibility is explored in the following section.

Two chemical processes could be responsible for the gradient in $\mathcal{R}$: isotope-selective photodissociation (ISPD) and chemical fractionation. ISPD can lower the ^{13}CO abundance relative to CO in the nucleus since the rarer isotope is less shielded from destructive radiation. ISPD requires a strong, localized source of ultraviolet radiation, and clumpiness to maximize the surface area of the clouds while maintaining the high observed column densities. The nuclei of nearly all the survey galaxies exhibit high far-infrared (FIR) luminosities indicative of massive star formation, so sources of dissociating photons exist. ISPD would produce CO/C^{18}O intensity ratios even higher than $\mathcal{R}$ since the C^{18}O optical depth is lower than that of ^{13}CO. Nine galaxies have CO, ^{13}CO and C^{18}O emission observed at roughly the same resolution as this work (Casoli et al. 1992b; Aalto et al. 1991; Sage et al. 1991), and there is a strong correlation between $\mathcal{R}$ and the CO/C^{18}O intensity ratio (Figure 6). However, there is no corresponding positive correlation between $\mathcal{R}$ and ^{13}CO/C^{18}O. In addition, ^{13}CO/C^{18}O stays the same or even *decreases* when viewed with higher resolution in NGC 253 and M82 (Harrison et al. 1999; Wild et al. 1992) while it should presumably be highest near the central ionizing sources. In fact in M82 at 13″ resolution, the highest ^{13}CO/C^{18}O ratio is found toward the weaker, eastern millimeter continuum source (Wild et al. 1992; Carlstrom & Kronberg 1991).

The C II/CO intensity ratio should be sensitive to the ultraviolet field strength and clumpiness of the gas (Stacey et al. 1991), and thus may also indicate the importance of ISPD. Figure 7 shows the central value of $\mathcal{R}$ for the survey galaxies plotted against this ratio. The linear correlation coefficient is less than 0.2, indicating a very low probability of correlation.

Fractionation in the disk could lower the CO column density relative to that of ^{13}CO by factors of a few, but would have little effect on $\mathcal{R}$ because of the high optical depth of the CO line. Also, this mechanism requires lower temperatures (< 30 K), and CO optical depths < 10 (e.g., Keene et al. 1998). The CO line strengths indicate substantial disk column densities ($> 10^{20}\,\mathrm{cm}^{-2}$), but if the gas is sufficiently clumpy, fractionation on individual clump surfaces may be possible. Whether the cloud temperatures in the disk are low enough to support large-scale fractionation is more difficult to determine. The temperatures of the central regions of all the survey galaxies are inferred to be high from multi-line observations of CO (Wall et al. 1993; Wild et al. 1992), C II spectra (Stacey et al. 1991), and IRAS

colors (e.g., Young et al. 1989), but little data for galactic disks exist. Studies of NGC 6946 and M51 indicate that higher gas temperatures in the disk are limited to the spiral arms and various hot spots (Engargiola 1991; Fitt et al. 1992; Madden et al. 1993; Tuffs et al. 1996). Little CO emission is seen outside of these warmer regions, where the gas might be cool enough to support fractionation.

To summarize, we eliminate nearly all arguments in favor of abundance variations as the cause of a gradient in $\mathcal{R}$. ISPD and CO enhancements due to gas transport or stellar nucleosynthesis are unlikely to be responsible for the observed gradients in $\mathcal{R}$ due to the high optical depth of CO, and the lack of expected gradients or correlations with other line ratios. Also the gradient in $\mathcal{R}$ in the Milky Way is in the opposite sense of the ^{12}C/^{13}C abundance gradient. It is difficult to test whether fractionation in the disk is important, though most of the CO emission in galactic disks is limited to relatively warm regions where it would not occur. Nuclear superwinds could effectively lower the beam-averaged ^{13}CO column density by creating very small clouds, which would result in higher values of $\mathcal{R}$ in starburst nuclei. This prediction is tested in the following section.

4.1.2. Cloud Properties

The CO/^{13}CO intensity ratio should be a straightforward measure of the ^{13}CO optical depth. For example in LTE, given optically thick CO emission and optically thin ^{13}CO emission, and that their emission comes from the same volume of gas,

$$I(\mathrm{CO})/I(^{13}\mathrm{CO}) \approx 1/\tau(^{13}\mathrm{CO}). \tag{1}$$

In this case, the mean optical depth of the gas in these galaxies generally decreases toward the nucleus. In LTE, $\tau \propto (N/\Delta v)/T_k^2$, for high T_k. Therefore, to produce the observed gradient in $\mathcal{R}$, the clouds in galactic nuclei are probably warmer, have lower column densities, and/or higher internal velocity dispersions.

To determine which cloud parameters dominate the variation in $\mathcal{R}$, and to include volume density as another important cloud parameter, we perform single-component model calculations of non-LTE CO excitation. We assume that the emission originates in unresolved, homogeneous, spherical clouds, and include a photon escape probability function to account for the radiative excitation of optically thick lines (Stutzki & Winnewisser 1985). The emission from the first 11 levels of CO is modeled. We use the collision rates of Flower & Launay (1985). The excitation of ^{13}CO is assumed to be identical to that of CO (cf., Wilson, Langer, & Goldsmith 1981), and the ^{13}CO line temperature is estimated by decreasing the

column density of CO by the [CO]/[^{13}CO] abundance ratio. Values of [CO]/[^{13}CO]=30–80 are considered.

Figure 8 shows the expected CO/^{13}CO intensity ratio from a cloud as a function of H_2 volume density ($n_{\mathrm{H_2}}$), CO column density per velocity interval ($N/\Delta v$), and kinetic temperature (T_k), given [CO]/[^{13}CO]=60. As expected, the ratio is a strong function of cloud column density and temperature, especially if the CO emission is thermalized. For example, a change in T_k from 10 to 30 K results in roughly a factor 3 variation in $\mathcal{R}$. For low densities, the optical depth of ^{13}CO is non-neglible, and the dependence on temperature diminishes (though a higher optical depth of the ^{13}CO line does not necessarily imply $\mathcal{R} \sim 1$ when LTE does not apply). Its dependence on density is weaker, especially for $T_k < 50$ K, and reflects the difference between subthermally excited and thermalized (near LTE) CO emission. Below $n_{\mathrm{H_2}} \sim 10^5$ cm^{-3}, $\mathcal{R}$ may vary by factors of a few with density, depending on T_k and $N/\Delta v$.

To test how variations in $N/\Delta v$ may affect the gradient in $\mathcal{R}$, we estimate the ratio of the column density within and outside of a 2 kpc radius in each galaxy. The column density per velocity interval for individual clouds, $N_c/\Delta v_c$ would have to decrease toward the nucleus to cause an increase in $\mathcal{R}$. We also assume a proportionality between the CO and ^{13}CO intensities and the beam-averaged column density, N, such that

$$\frac{(N_c/\Delta v_c)_{R<2\mathrm{kpc}}}{(N_c/\Delta v_c)_{R>2\mathrm{kpc}}} = \frac{(XI/\Delta v)_{R<2\mathrm{kpc}}}{(XI/\Delta v)_{R>2\mathrm{kpc}}}\Big(\frac{\phi_{R>2\mathrm{kpc}}}{\phi_{R<2\mathrm{kpc}}}\Big), \tag{2}$$

where ϕ is the beam filling factor, and we assume constant CO and ^{13}CO abundances. The velocity width is estimated from the full line width. $I/\Delta v$ rises toward the nuclei of each survey galaxy by factors of 2–30 using CO, and 1.3–7 using ^{13}CO. For individual clouds, $N_c/\Delta v_c$ could still decrease towards the nucleus if the beam filling factor rises faster than $XI/\Delta v$. In other words, if crowding in the nucleus is significant, then a higher value of $\mathcal{R}$ is still possible if $N_c/\Delta v_c$ of individual clouds there is lower than in the disk. Such increases in ϕ appear reasonable given the increase in line intensities and their likely dependence on varying excitation conditions from disk to nucleus. Therefore, we cannot eliminate the possibility of small nuclear clouds, such as would be produced by starburst winds, though the amount of variation in $N_c/\Delta v_c$ depends mostly on the internal turbulence of the clouds and the change in excitation conditions, that is, the variation in volume and column density and kinetic temperature.

An increase in the gas volume density toward the nucleus can contribute to the gradient in $\mathcal{R}$. For certain conditions ($T_k > 10$ K, $n_{\mathrm{H_2}} \sim 10^3$–$10^5$ cm^{-3}), an increase in density of an order of magnitude can double $\mathcal{R}$. The centers of galaxies are known to have enhanced gas

densities (Wall et al. 1993; Helfer & Blitz 1993; Paglione et al. 1997). Figure 7 shows the central value of $\mathcal{R}$ for the survey galaxies plotted against the (HCN $J=3\rightarrow2$)/(HCN $J=1\rightarrow0$) intensity ratio, which is sensitive to the gas density (Paglione et al. 1997). A positive trend is apparent, though there is no significant correlation (the linear correlation coefficient is 0.2).

The correlation between $\mathcal{R}$ and IRAS color temperature (the ratio of global fluxes at 60 and 100μm) is well established (Young & Sanders 1986; Aalto et al. 1991; Sage & Isbell 1991; Taniguchi et al. 1999). There is a good correlation between $\mathcal{R}$ and color temperature for the galaxies presented here as well. According to the homogeneous cloud model, $\mathcal{R}$ varies with the gas kinetic temperature also, especially for $n_{\mathrm{H}_2} > 10^3$ cm^{-3}. Generally $\mathcal{R} \propto T_k^{1.4}$ for high densities, and $\mathcal{R} \propto T_k^{0.3}$ for $n_{\mathrm{H}_2} < 10^3$ cm^{-3}. Such a strong dependence on temperature, especially in combination with the expected increase in density towards the nucleus, suggests that most if not all of the variation seen in $\mathcal{R}$ is due to the high gas temperatures in these (mostly starburst) galactic nuclei. Figure 7 shows the central value of $\mathcal{R}$ for the survey galaxies plotted against the (CO $J=3\rightarrow2$)/(CO $J=1\rightarrow0$) intensity ratio, which is generally sensitive to T_k. A linear correlation coefficient of 0.5 indicates a significant correlation between these ratios.

A two-component model can also explain a rise in $\mathcal{R}$ at the nucleus without gradients in the bulk physical conditions of the clouds. We test a model where the cloud properties do not change, but warm and diffuse gas (n_{H_2} = 100 cm^{-3}, T_k = 30 K) is added to the nucleus. Given the observed CO/^{13}CO ratios in galactic disks, a diffuse component with twice the beam filling factor of the dense component provides enhancements in $\mathcal{R}$ as high as 90% for very low temperatures ($T_k < 20$ K). Enhancements of 10–50%, for T_k = 20–75 K and $n_{\mathrm{H}_2} \sim 10^2$–$10^4$cm^{-3}, are more likely and still match the observed gradients in $\mathcal{R}$. Decrements in $\mathcal{R}$ of up to 20–40% can also be produced by including the diffuse component, but require that the dense component be very dense and warm ($n_{\mathrm{H}_2} > 10^4$ cm^{-3}, $T_k > 50$ K), which are unlikely conditions in galactic disks.

To summarize, the observed gradient in $\mathcal{R}$ can be successfully explained by a gradient in the gas kinetic temperature. Increased volume densities in the nucleus may also contribute to raising $\mathcal{R}$ there. The column densities of individual clouds may decrease enough to cause the observed gradient in $\mathcal{R}$, though this variation may be secondary to changes in temperature. This result is expected since in the LTE limit, the optical depth of ^{13}CO, which is inversely proportional to $\mathcal{R}$, depends more strongly on T_k. Therefore a modest rise in T_k towards the nucleus (e.g., from 10 K to 30 K, see Figure 8) can easily account for the gradient in $\mathcal{R}$. Finally, a two-component model with warm and diffuse gas in the nucleus can reproduce the observed enhancements in $\mathcal{R}$ for a reasonable range of temperatures and densities. However,

the observed decrements in $\mathcal{R}$ are more difficult to explain with this model.

4.1.3. X-Factor

A positive gradient in the X-factor has been suggested for the Galaxy (Digel et al. 1990; Sodroski et al. 1995; Dahmen et al. 1998). This result would follow naturally from the gradient in $\mathcal{R}$ found in this survey and the Milky Way. That is, the H_2 mass estimated from a direct proportionality with CO intensity would overestimate the true mass in galactic centers, which is presumably traced less ambiguously by the more optically thin ^{13}CO emission. Despite the probable Galactic gradient in the X-factor, the apparently strong dependence of $\mathcal{R}$ on cloud properties (and possibly chemical abundances) indicates that many things can contribute to varying the proportionality between I_{CO} and H_2 column density. Using the homogeneous cloud model from the previous section, as expected, $\mathcal{R}$ increases as X decreases given a constant CO abundance. Therefore, we suggest that a variable X-factor results from the same processes that affect $\mathcal{R}$. Determining unambiguous variations in X requires a better understanding of the many physical processes that can affect $\mathcal{R}$.

We estimate the H_2 column densities inside and outside a 2 kpc radius in the survey galaxies using various means: from the CO intensity and the standard, constant X-factor of $1.6\times10^{20}\,\mathrm{cm}^{-2}\,(\mathrm{K\ km\,s}^{-1})^{-1}$; from the ^{13}CO intensity, assuming optically thin emission and LTE; and from the homogeneous cloud model, which includes non-LTE excitation and radiative trapping.

The molecular masses inside a 2 kpc radius, derived from the standard X-factor, are listed in Table 3. For most of the galaxies, the mass derived from CO is less than the dynamical mass inside 2 kpc. However for IC 342, M82 and NGC 6946, it is comparable to the dynamical mass. Unlike M82, IC 342 and NGC 6946 have typical CO/^{13}CO intensity ratios.

The H_2 column density can be estimated from the ^{13}CO intensity assuming optically thin emission and LTE using

$$N_{\mathrm{H}_2} = 4.2\times10^{19} T_k e^{2.645/T_k} I(^{13}\mathrm{CO}), \tag{3}$$

where the ^{13}CO abundance is $8\times10^{-5}/60$ (Frerking, Langer, & Wilson 1982). Masses derived from equation 3 are listed in Table 3 for $T_k = 10$ K and 50 K. For most of the survey galaxies, these masses are similar to those derived from the standard X-factor and CO, which implies that the kinetic temperature is between 10 and 50 K. In fact, the gas kinetic temperature

can be estimated by setting the column densities derived from both CO and ^{13}CO. The temperatures inside 2 kpc (Table 3) are 20–60 K, and only somewhat lower in the disk. The higher temperatures are quite high compared to those derived from radiative transfer analyses (Wall et al. 1993), and seem unlikely over such large areas, especially in galactic disks. That this temperature seems high indicates that the masses derived from ^{13}CO are generally lower than those derived from CO.

We estimate column densities with the homogeneous cloud model assuming $n_{\rm H_2} = 300$ cm^{-3} and $T_k = 10$ K in the disk, and $n_{\rm H_2} = 10^4$ cm^{-3} and $T_k = 30$–50 K within a 2 kpc radius. We use the CO/^{13}CO intensity ratios given in Table 2. Assuming LTE and optically thin ^{13}CO emission, the kinetic temperature is overestimated on average by a factor of 3–4 in the disk, and underestimated by 2.3–3 times in the nucleus. The average conversion factor in the disk is $(1$–$3)\times10^{20}\,{\rm cm^{-2}\,(K\,km\,s^{-1})^{-1}}$, which is consistent with the value in the disk of the Milky Way. For the nuclei we find $X = (0.4$–$1.4)\times10^{20}\,{\rm cm^{-2}\,(K\,km\,s^{-1})^{-1}}$, which is factors of 2–5 times lower than in the disk, and 1.2–3.3 times lower than the standard Galactic value. Using the standard Galactic X-factor in galactic nuclei could therefore overestimate the true mass by factors of a few. Note that the model indicates that the X-factor is always smaller in galactic nuclei, regardless of the gradient in $\mathcal{R}$.

5. Conclusions

We observed the CO and ^{13}CO $J = 1 \rightarrow 0$ emission along the major axes of 17 nearby galaxies. On average, the CO/^{13}CO intensity ratio, $\mathcal{R}$, inside a 2 kpc radius is roughly 30% higher than in the disk. This ratio is sensitive to variations in temperature and column density, as well as fractionation and isotope-selective photodissociation. Winds and gas inflow caused by mergers have also been suggested to vary $\mathcal{R}$, along with abundance variations due to stellar processing. We eliminate most mechanisms except for fractionation and variations in kinetic temperature, cloud column density and H_2 volume density. The gradient is most likely caused by the higher temperatures (and perhaps densities) typical of the central regions of starburst galaxies. Small nuclear clouds, perhaps caused by starburst superwinds, may also contribute to the variation in $\mathcal{R}$. We estimate that the X-factor ($X = N_{\rm H_2}/I_{CO}$) decreases toward galactic nuclei, as seen in the Milky Way, and its variation results from the same physical processes that affect $\mathcal{R}$. A modest increase in global gas temperatures easily accounts for the observed variation in $\mathcal{R}$, as well as a decrease in X of factors of 2–5, from disk to nucleus.

The FCRAO is operated through National Science Foundation grant AST 88-15406 and

with the permission of the Metropolitan District Commission. This work was also supported in part by grant 211290-5-25875E from the Consejo Nacional de Ciencia y Tecnología. The authors are grateful to M. Skrutski and the UMass Society of Physics Students for their support and help with recruiting interested young scientists. We also thank M. Belniak, N. Bouch, H. Cameron, N. Cartel, N. Durham, M. Gruol, S. Litchfield, J. Perry, S. Stephan, M. Thorn and R. White for their assistance with the observations. M. Richard and M. Goldstein thank the Five College Astronomy Department and the FCRAO for summer internships. T. Paglione gratefully acknowledges the generous hospitality of A. Lovell and D. Smith.

Table 1. Properties of Survey Galaxies and Maps.

Galaxy	R.A. (2000) h m s	Decl. (2000) ° ′ ″	V_{LSR}[a] (km s^{-1})	D (Mpc)	Map P.A. (degrees)	d[b] (kpc)	Map Size[c] (kpc)
NGC 253	00 47 35.1	−25 17 20	230	3	54	0.7	9.3
NGC 1068	02 42 40.7	−00 00 48	1150	14.4	90	3.2	20.1
IC 342	03 46 49.7	68 05 45	30	4	0	0.9	15.9
UGC 2855	03 48 22.6	70 07 57	1200	20	92	4.5	30.1
NGC 2146	06 18 37.6	78 21 19	920	14	128	3.1	13.5
M82	09 55 54.0	69 40 57	250	3.25	65	0.72	8.4
NGC 3079	10 01 58.2	55 40 42	1150	20	164	4.5	27.9
NGC 3184	10 18 17.2	41 25 26	590	13	135	2.9	23.7
NGC 3556	11 11 31.8	55 40 14	700	10	80	2.2	15.0
NGC 3593	11 14 36.0	12 49 06	600	9	90	2.0	12.6
NGC 3627	11 20 14.4	12 59 42	740	6.7	0	1.5	12.2
NGC 3628	11 20 16.2	13 35 22	850	6.7	103	1.5	15.1
NGC 4527	12 34 08.8	02 39 13	1770	15	67	3.3	20.9
NGC 4631	12 42 07.6	32 32 28	630	9	88	2.0	13.5
NGC 5055	13 15 49.2	42 02 06	500	7	105	1.6	15.8
M51	13 29 53.2	47 11 48	450	9.6	0	2.1	21.6
NGC 6946	20 34 51.8	60 09 15	50	10	45	2.2	22.5

[a]Central position

[b]Linear extent of 46″ at distance D

[c]Full extent of map along major axis, sampled every 22.″14 with a 46″ beam (FWHM).

Table 2. Variation of CO/^{13}CO Intensity Ratio.

Galaxy	$I(\mathrm{CO})/I(^{13}\mathrm{CO})^a$				Ratio^b
	$R < 23''$	$R > 23''$	$R < 2$ kpc	$R > 2$ kpc	
NGC 253	11.9 ± 0.5 ± 3.4	8.8 ± 0.5	12.4 ± 0.5	6.9 ± 0.8	1.8 ± 0.2
NGC 1068	10.7 ± 0.6 ± 1.9	11.7 ± 1.2	10.4 ± 0.4	11.6 ± 1.1	0.9 ± 0.1
IC 342	8.4 ± 0.5 ± 1.6	7.1 ± 0.6	10.8 ± 0.8	6.4 ± 0.6	1.7 ± 0.2
UGC 2855	11.7 ± 1.7 ± 2.3	9.4 ± 1.7	11.7 ± 1.7	9.4 ± 1.7	1.2 ± 0.3
NGC 2146	14.9 ± 1.3 ± 8.6	28.1 ± 6.9	15.5 ± 1.1	22.8 ± 4.5	0.7 ± 0.1
M82	27.3 ± 1.0 ± 7.8	12.9 ± 0.5	20.9 ± 0.7	12.1 ± 6.9	1.7 ± 1.0
NGC 3079	15.3 ± 1.8 ± 5.1	10.1 ± 2.1	15.3 ± 1.8	10.1 ± 2.1	1.5 ± 0.4
NGC 3184	4.9 ± 1.2 ± 2.3	4.4 ± 0.8	5.6 ± 1.1	4.0 ± 0.6	1.4 ± 0.3
NGC 3556	8.7 ± 1.4 ± 5.6	6.8 ± 0.6	7.0 ± 0.8	6.9 ± 0.7	1.0 ± 0.2
NGC 3593	10.6 ± 2.2 ± 10	11.4 ± 3.2	16.8 ± 4.6	5.7 ± 2.3	2.9 ± 1.4
NGC 3627	11.2 ± 1.2 ± 5.7	17.4 ± 2.1	15.5 ± 1.6	17.8 ± 4.1	0.9 ± 0.2
NGC 3628	9.2 ± 0.4 ± 2.3	10.3 ± 0.6	9.7 ± 0.4	11.2 ± 1.1	0.9 ± 0.1
NGC 4527	6.1 ± 0.5 ± 1.4	6.9 ± 0.8	6.7 ± 0.9	6.7 ± 0.6	1.0 ± 0.2
NGC 4631	16.3 ± 2.4 ± 9.9	9.1 ± 0.7	13.1 ± 1.3	8.4 ± 0.9	1.6 ± 0.2
NGC 5055	5.7 ± 0.6 ± 3.1	8.2 ± 0.7	7.1 ± 0.6	9.2 ± 1.1	0.8 ± 0.1
M51	5.4 ± 0.4 ± 1.0	7.5 ± 0.6	6.4 ± 0.4	8.2 ± 0.9	0.8 ± 0.1
NGC 6946	17.0 ± 1.4 ± 6.6	10.4 ± 1.1	12.7 ± 1.0	9.8 ± 1.4	1.3 ± 0.2
Average	11.5 ± 0.3 ± 1.4	10.6 ± 0.5	11.6 ± 0.4	9.8 ± 0.6	1.3 ± 0.1

[a]From weighted averages of data within or beyond noted radii. For the central position, the estimated systematic uncertainty is listed after the statistical uncertainty.

[b]Intensity ratio inside 2 kpc divided by that outside of 2 kpc. Uncertainty is based on the statistical uncertainty.

Table 3. Modeling Results^{a}.

Galaxy	M_{H_2}(CO)	M_{H_2}(^{13}CO)		T_k (K)		X	
		$T_k = 10$ K	$T_k = 50$ K	$R < 2$ kpc	$R > 2$ kpc	$R < 2$ kpc	$R > 2$ kpc
NGC 253	2.40 (0.04)	0.66 (0.03)	2.7 (0.1)	45 (2)	23 (3)	$0.5^{+0.4}_{-0.2}$	$2.5^{+1.5}_{-0.7}$
NGC 1068	2.16 (0.32)	0.75 (0.10)	3.0 (0.4)	37 (2)	42 (4)	$0.7^{+0.2}_{-0.2}$	$1.1^{+0.4}_{-0.3}$
IC 342	0.99 (0.16)	0.32 (0.03)	1.3 (0.1)	39 (3)	22 (2)	$0.6^{+0.3}_{-0.2}$	$2.8^{+0.9}_{-0.7}$
UGC 2855	0.87 (0.03)	0.25 (0.04)	1.0 (0.1)	42 (7)	33 (6)	$0.6^{+0.3}_{-0.2}$	$1.6^{+0.5}_{-0.4}$
NGC 2146	1.47 (0.29)	0.34 (0.09)	1.4 (0.4)	56 (4)	84 (17)	$0.4^{+1.0}_{-0.3}$	$0.4^{+1.1}_{-0.2}$
M82	2.83 (0.01)	0.46 (0.01)	1.9 (0.1)	77 (3)	44 (26)	$0.3^{+0.2}_{-0.1}$	$1.1^{+0.7}_{-0.4}$
NGC 3079	1.87 (0.02)	0.42 (0.05)	1.7 (0.2)	56 (7)	36 (8)	$0.4^{+0.4}_{-0.2}$	$1.4^{+1.1}_{-0.5}$
NGC 3184	0.16 (0.01)	0.09 (0.02)	0.4 (0.1)	19 (4)	13 (2)	$1.5^{+2.9}_{-0.7}$	$4.9^{+8.5}_{-1.8}$
NGC 3556	0.34 (0.01)	0.17 (0.02)	0.7 (0.1)	24 (3)	23 (3)	$1.1^{+5.0}_{-0.6}$	$2.5^{+8.7}_{-1.3}$
NGC 3593	0.50 (0.04)	0.10 (0.03)	0.4 (0.1)	61 (17)	19 (9)	> 0.1	> 1.2
NGC 3627	0.81 (0.01)	0.18 (0.02)	0.7 (0.1)	57 (6)	65 (15)	$0.4^{+0.7}_{-0.3}$	$0.5^{+1.2}_{-0.2}$
NGC 3628	1.47 (0.02)	0.52 (0.02)	2.1 (0.1)	34 (2)	40 (4)	$0.7^{+0.5}_{-0.3}$	$1.2^{+0.6}_{-0.4}$
NGC 4527	1.03 (0.10)	0.49 (0.12)	2.0 (0.5)	23 (3)	23 (2)	$1.2^{+0.8}_{-0.4}$	$2.6^{+1.2}_{-0.7}$
NGC 4631	0.83 (0.02)	0.22 (0.02)	0.9 (0.1)	47 (5)	29 (3)	$0.5^{+2.0}_{-0.3}$	$1.8^{+7.1}_{-1.0}$
NGC 5055	0.57 (0.02)	0.27 (0.02)	1.1 (0.1)	25 (2)	32 (4)	$1.1^{+2.5}_{-0.5}$	$1.6^{+3.0}_{-0.8}$
M51	1.16 (0.02)	0.62 (0.04)	2.5 (0.2)	22 (2)	29 (4)	$1.3^{+0.7}_{-0.4}$	$1.9^{+0.7}_{-0.4}$
NGC 6946	1.79 (0.03)	0.48 (0.04)	2.0 (0.1)	46 (4)	35 (5)	$0.5^{+0.5}_{-0.3}$	$1.5^{+1.5}_{-0.6}$

[a]Uncertainty given in parentheses.

Column 1: Galaxy

Column 2: Mass inside 2 kpc from standard conversion factor and I(CO) in $10^9\ M_\odot$

Columns 3 and 4: Mass inside 2 kpc from ^{13}CO (eq. 3) for given T_k in $10^9\ M_\odot$

Columns 5 and 6: T_k from standard X-factor and column density estimated from ^{13}CO (eq. 3)

Columns 7 and 8: X-factor from non-LTE calculations and $\mathcal{R}$ (Table 2) in 10^{20} cm^{-2}(K km s^{-1})$^{-1}$

REFERENCES

Aalto, S., Black, J. H., Johansson, L. E. B., & Booth, R. S. 1991, A&A, 249, 323

Carlstrom, J. E. & Kronberg, Philipp P. 1991, ApJ, 366, 422

Carpenter, J. M., Snell, R. L., & Schloerb, F. P. 1990, ApJ, 362, 147

Carral, P., Hollenbach, D. J., Lord, S. D., Colgan, S. W. J., Haas, M. R., Rubin, R. H., Erickson, E. F. 1994, ApJ, 423, 223

Casoli, F., Dupraz, C., & Combes, F. 1992, A&A, 264, 55

Casoli, F., Dupraz, C., & Combes, F. 1992, A&A, 264, 49

Dahmen, G., Hüttemeister, S., Wilson, T. L., & Mauersberger, R. 1998, A&A, 331, 959

Dame, T. M., Hartmann, D., & Thaddeus, P. 2001, ApJ, 547, 792

Dickman, R. L., Snell, R. L., & Schloerb, F. P. 1986, ApJ, 309, 326

Digel, S., Bally, J., & Thaddeus, P. 1990, ApJ, 357, L29

Engargiola, G. 1991, ApJS, 76, 875

Erickson, N. R., Grosslein, R. M., Erickson, R. B., & Weinreb, S. 1999, IEEE Trans. Microwave Theory Tech., 47, 2212-2219

Fitt, A. J., Howarth, N. A., Alexander, P., Lazenby, A. N. 1992, MNRAS, 255, 146

Flower, D. R., & Launay, J. M. 1985, MNRAS, 214, 271

Frerking, M. A., Langer, W. D., & Wilson, R. W. 1982, ApJ, 262, 590

Friedli, D., Benz, W., & Kennicutt, R. 1994, ApJ, 430, L105

Garcia-Burillo, S., Guelin, M., Cernicharo, J. 1993, A&A, 274, 123

Harrison, A., Henkel, C., & Russell, A. 1999, MNRAS, 303, 157

Helfer, T. T. & Blitz, L. 1993, ApJ, 419, 86

Henkel, C. & Mauersberger, R. 1993, A&A, 274, 730

Hunter, S. D. et al. 1997, ApJ, 481, 205

Jog, C. J., & Das, M. 1992, ApJ, 400, 476

Keene, J., Schilke, P., Kooi, J., Lis, D. C., Mehringer, D. M., Phillips, T. G. 1998, ApJ, 494, L107

Kikumoto, T., Taniguchi, Y., Nakai, N., Matsushita, S., Kawabe, R. 1998, PASJ, 50, 309

Langer, W. D. & Penzias, A. A. 1990, ApJ, 357, 477

Lee, Y., Snell, R. L. & Dickman, R. L. 1990, ApJ, 355, 536

Loiseau, N., Reuter, H.-P., Wielebinski, R., & Klein, U. 1988, A&A, 200, L1

Madden, S. C., Geis, N., Genzel, R., Herrmann, F., Jackson, J., Poglitsch, A., Stacey, G. J., & Townes, C. H. 1993, ApJ, 407, 579

Mauersberger, R., Henkel, C., Walsh, W., Schulz, A. 1999, A&A, 341, 256

Oka, T., Hasegawa, T., Sato, F., Tsuboi, M., Miyazaki, A. 1998, ApJS, 118, 455

Paglione, T. A. D., Jackson, J. M., Ishizuki, S. 1997, ApJ, 484, 656

Papadopoulos, P. P. & Seaquist, E. R. 1999, ApJ, 516, 114

Polk, K. S., Knapp, G. R., Stark, A. A., & Wilson, R. W. 1988, ApJ, 332, 432

Rickard, L. J. & Blitz, L. 1985, ApJ, 292, L57

Sage, L. J. & Isbell, D. W. 1991, A&A, 247, 320

Sage, L. J., Henkel, C., & Mauersberger, R. 1991, A&A, 249, 31

Sakamoto, S. 1996, ApJ, 462, 215

Sodroski, T. J. 1991, ApJ, 366, 95

Sodroski, T. J., et al. 1995, ApJ, 452, 262

Solomon,, P. M., Sanders, D. B. & Scoville, N. Z. 1979, ApJ, 232, 89

Stacey, G. J., Geis, N., Genzel, R., Lugten, J. B., Poglitsch, A., Sternberg, A., & Townes, C. H. 1991, ApJ, 373, 423

Stark, A. A. & Carlson, E. R. 1982, ApJ, 279, 122

Stutzki, J., & Winnewisser, G. 1985, A&A, 144, 13

Taniguchi, Y., Ohyama, Y., & Sanders, D. B. 1999, ApJ, 522, 214

Tuffs, R. J., Lemke, D., Xu, C., Davies, J. J., Gabriel, C., Heinrichsen, I., Helou, G., Hippelein, H., Lu, N. Y., Skaley, D. 1996, A&A, 315, L149

Wall, W. F., Jaffe, D. T., Bash, F. N., Israel, F. P., Maloney, P. R., & Baas, F. 1993, ApJ, 414, 98

Wielebinski, R., Dumke, M. & Nieten, Ch. 1999, A&A, 347, 634

Wild, W., Harris, A. I., Eckart, A., Genzel, R., Graf, U. U., Jackson, J. M., Russell, A. P. G., & Stutzki, J. 1992, A&A, 265, 447

Wilson, R. W., Langer, W. D., & Goldsmith, P. F. 1981, ApJ, 243, L47

Young, J. S. & Sanders, D. B. 1986, ApJ, 302, 680

Young, J. S. & Scoville, N. Z. 1982, ApJ, 258, 467

Young, J. S., Xie, S., Kenny, J. D. P., and Rice, W. L. 1989, ApJS, 70, 699

Young, J. S., Xie, S., Tacconi, L., Knezek, P., Viscuso, P., Tacconi-Garman, L., Scoville, N., Schneider, S., Schloerb, F. P., Lord, S., Lesser, A., Kenney, J., Huang, Y.-L., Devereux, N., Claussen, M., Case, J., Carpenter, J., Berry, M., & Allen, L. 1995, ApJS, 98, 219

Fig. 1.— Spectra of CO (heavy lines) and ^{13}CO (light lines) emission for the survey galaxies. Except for IC 342, all ^{13}CO spectra are smoothed to 27.2 $\mathrm{km\,s^{-1}}$ resolution for display. The temperature scale is for the ^{13}CO line. The CO line is divided by 10 for display.

Fig. 2.— The CO and ^{13}CO integrated intensities ($\int T_A^* dv$), and their ratios, versus position along the major axis. Upper and lower limits (3σ) are denoted with downward- and upward-pointing triangles, respectively. Error bars are 1σ statistical estimates based on the r.m.s. noise, line width and channel width.

Fig. 3.— The CO/^{13}CO intensity ratio as a function of position. The data are folded about the nucleus and binned to make the uncertainty in $\mathcal{R}$ uniform along the major axis. Vertical error bars indicate the statistical uncertainties of the data (see text). Horizontal bars indicate the bin sizes.

Fig. 4.— Comparison of the ratio of CO and ^{13}CO integrated intensities inside and outside of selected radii: $23''$ (beam HWHM), 1, 1.5 and 2 kpc. The lines indicate slopes of 2/3, 1, 3/2, 2 and 4 (dash-triple-dot, solid, dashed, dash-dot and dotted, respectively).

Fig. 5.— Same as Figure 4 indicating the variation in the gradient of $\mathcal{R}$ with the size of the central region. The ratios for M82 are divided by 10 for clarity. The filled symbol denotes the ratio for the central point without binning. The other connected points are for central regions of 1, 1.5 and 2 kpc radii, in sequence.

Fig. 6.— Central CO/^{13}CO intensity ratio plotted against the central CO/C^{18}O and ^{13}CO/C^{18}O intensity ratios. All data are at similar resolution, $\sim 45''$. References - NGC 253, IC 342, M82: this work, Sage et al. (1991); NGC 1808, NGC 2146, NGC 4826, Circinus, NGC 7552: this work, Aalto et al. (1991); NGC 3256: Casoli et al. (1992b).

Fig. 7.— Central CO/^{13}CO intensity ratio plotted against C II/CO (Stacey et al. 1991; Carral et al. 1994), HCN $J=3\rightarrow 2/J=1\rightarrow 0$ (Paglione et al. 1997), and CO $J=3\rightarrow 2/J=1\rightarrow 0$ (Mauersberger et al. 1999; Papadopoulos & Seaquist 1999; Wielebinski, Dumke & Nieten 1999). Error bars denote systematic uncertainties.

Fig. 8.— Expected CO/^{13}CO intensity ratios as functions of kinetic temperature, CO column density per velocity interval, and H_2 volume density.

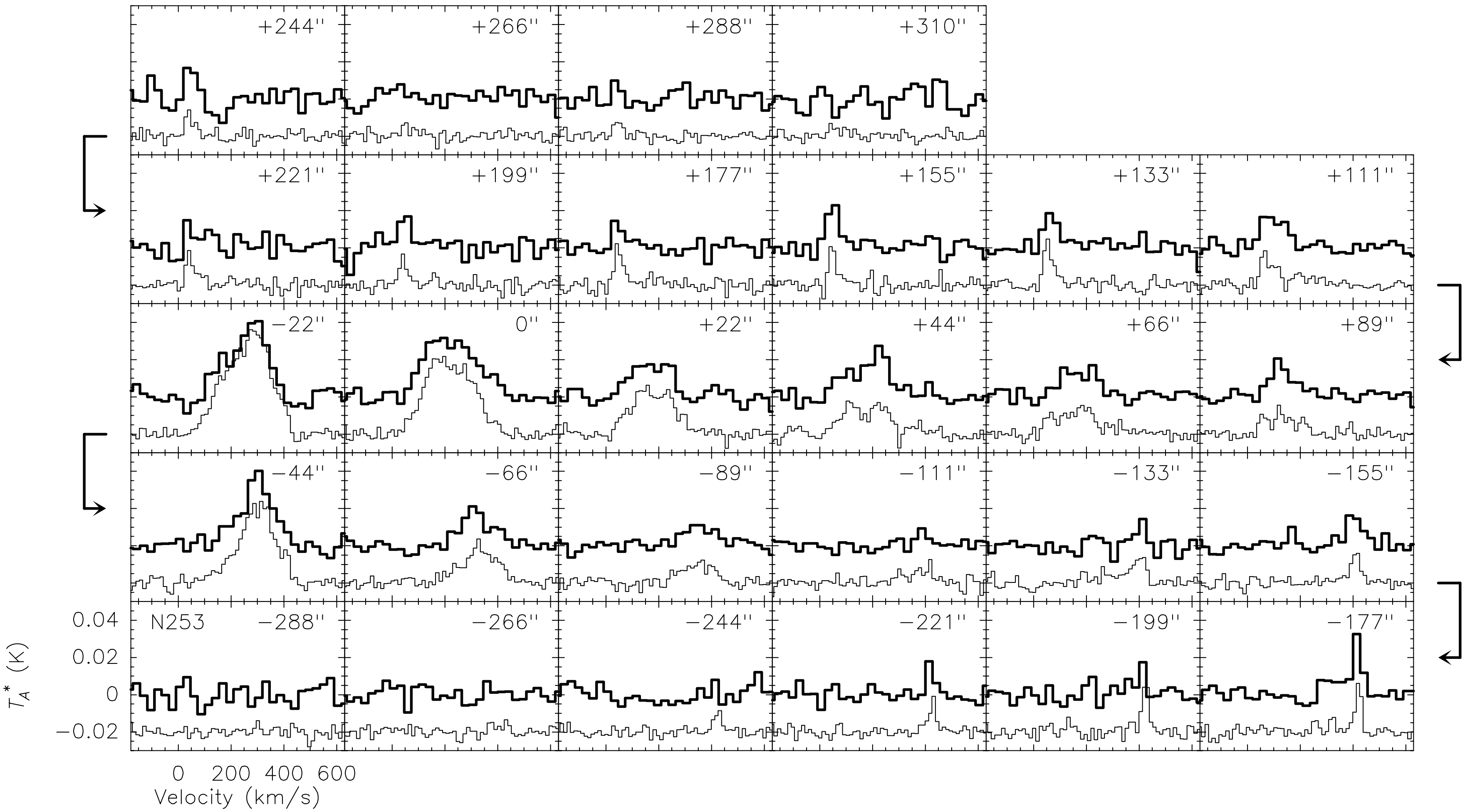
+244''
+266''
+288''
+310''
+221''
+199''
+177''
+155''
+133''
+111''
−22''
0''
+22''
+44''
+66''
+89''
−44''
−66''
−89''
−111''
−133''
−155''
N253
−288''
−266''
−244''
−221''
−199''
−177''
0.04
0.02
0
−0.02
T_A^* (K)
0 200 400 600
Velocity (km/s)

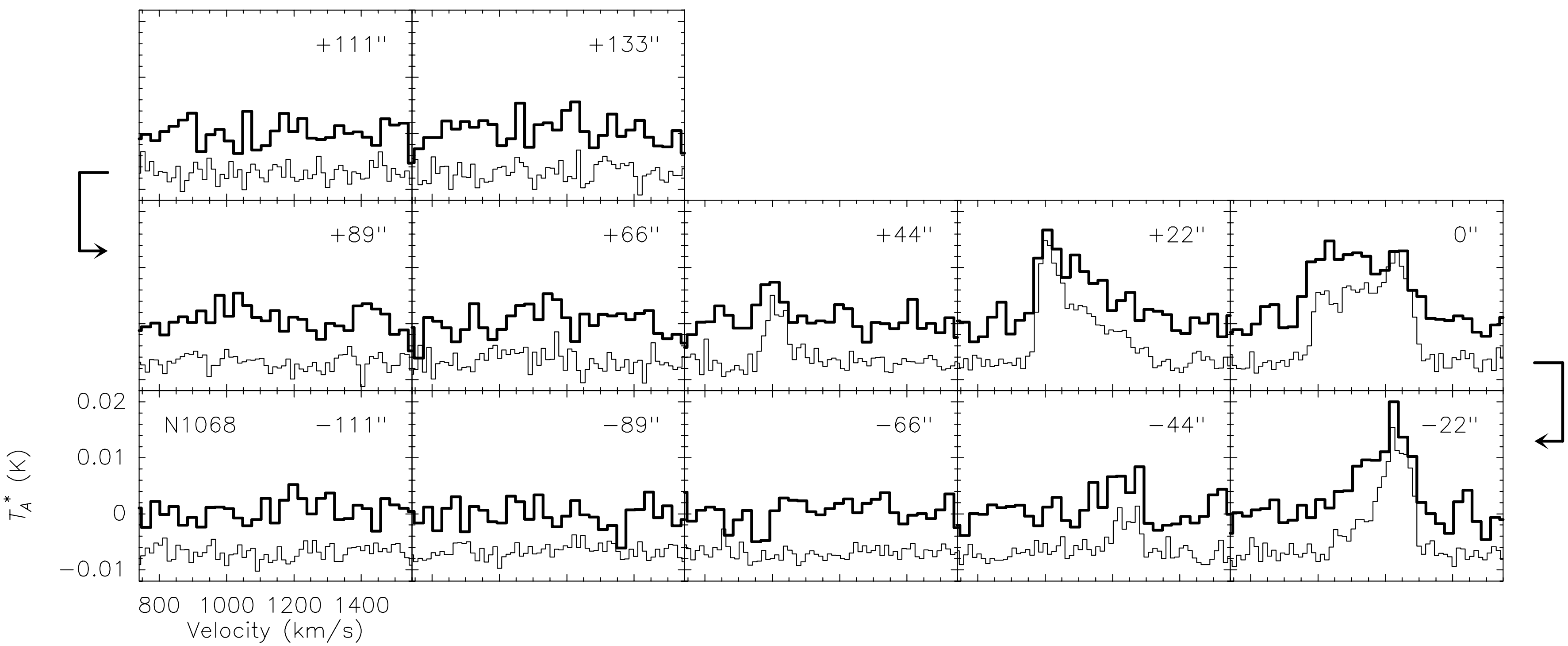

+111''
+133''
+89''
+66''
+44''
+22''
0''
N1068
−111''
−89''
−66''
−44''
−22''
0.02
0.01
0
−0.01
T_A^* (K)
800 1000 1200 1400
Velocity (km/s)

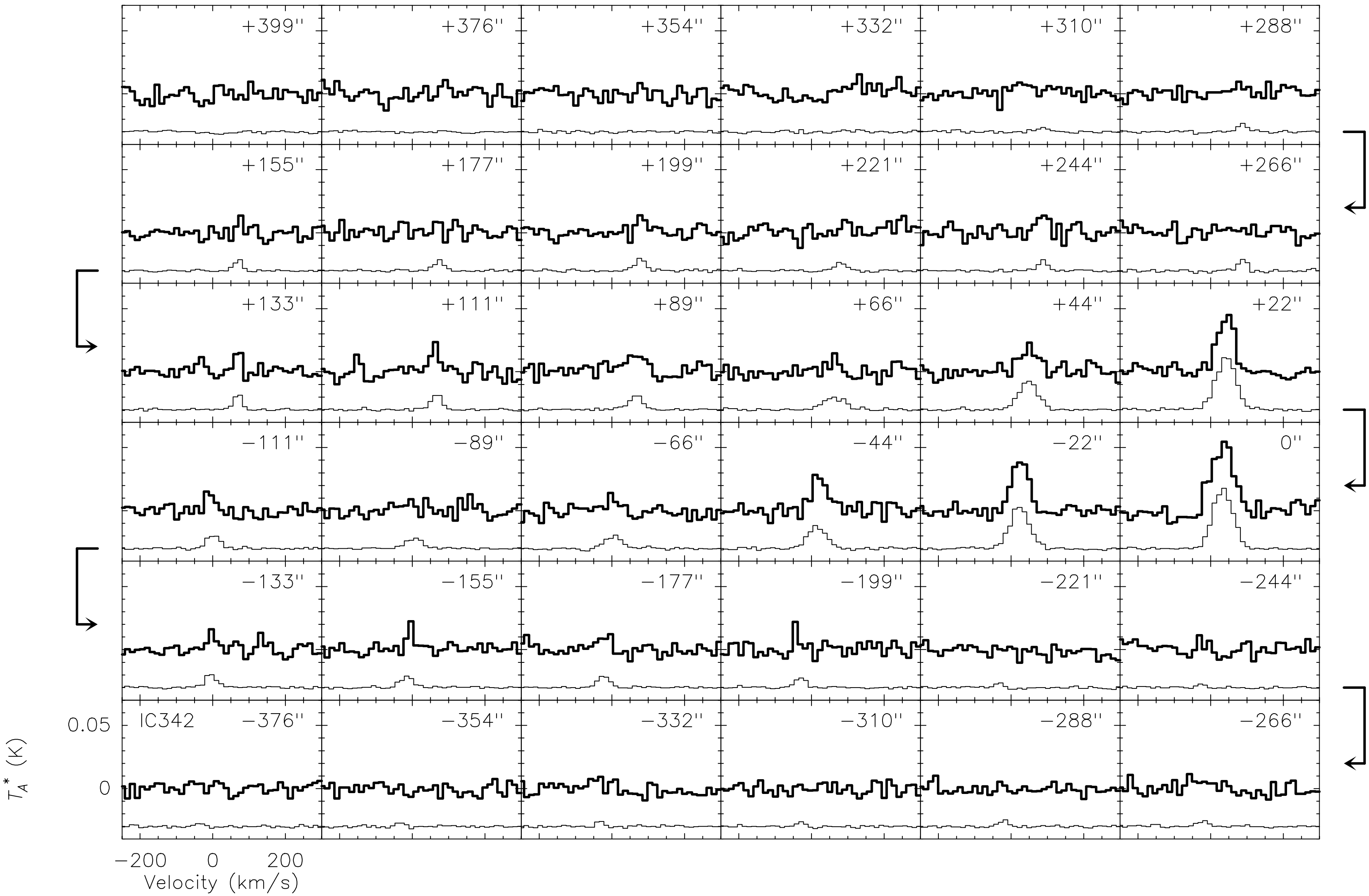

+399''
+376''
+354''
+332''
+310''
+288''
+155''
+177''
+199''
+221''
+244''
+266''
+133''
+111''
+89''
+66''
+44''
+22''
−111''
−89''
−66''
−44''
−22''
0''
−133''
−155''
−177''
−199''
−221''
−244''
IC342
−376''
−354''
−332''
−310''
−288''
−266''
0.05
0
T_A^* (K)
−200
0
200
Velocity (km/s)

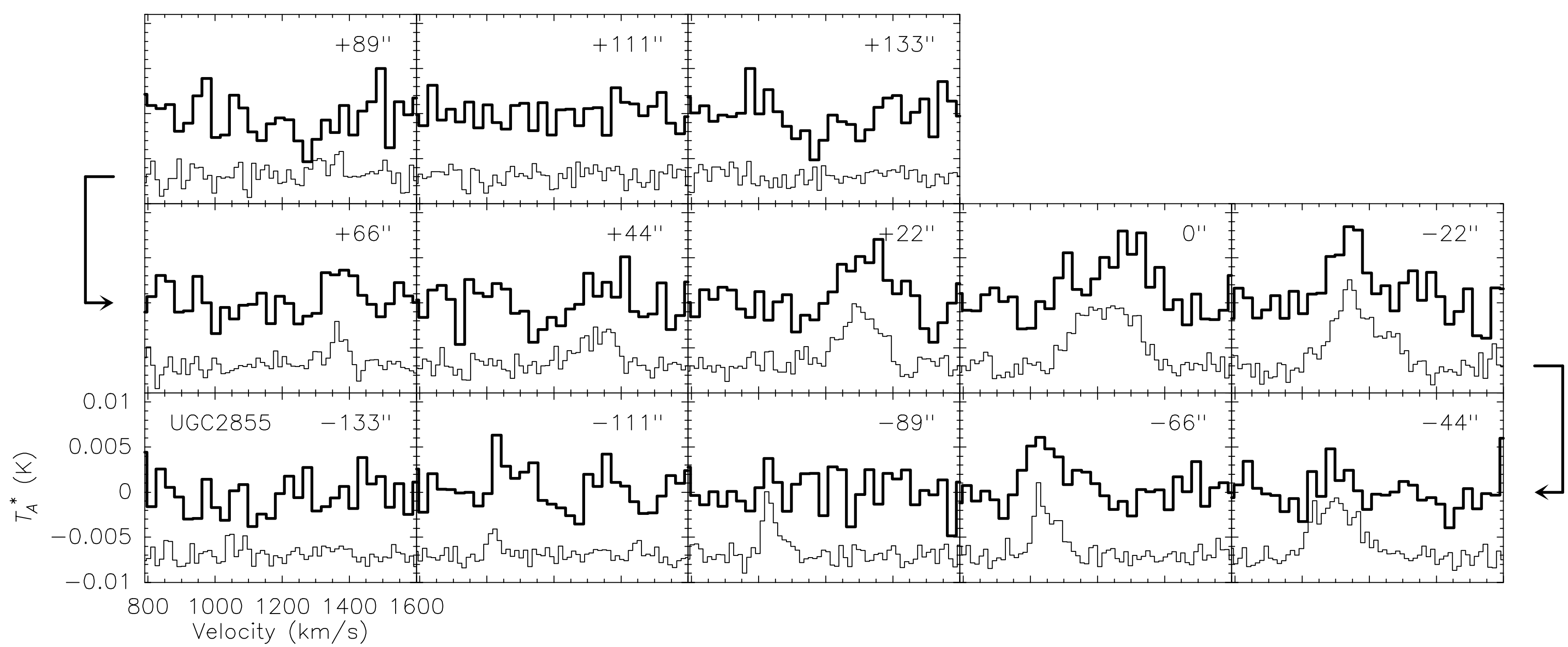

+89''
+111''
+133''
+66''
+44''
+22''
0''
−22''
UGC2855
−133''
−111''
−89''
−66''
−44''
0.01
0.005
0
−0.005
−0.01
T_A^* (K)
800 1000 1200 1400 1600
Velocity (km/s)

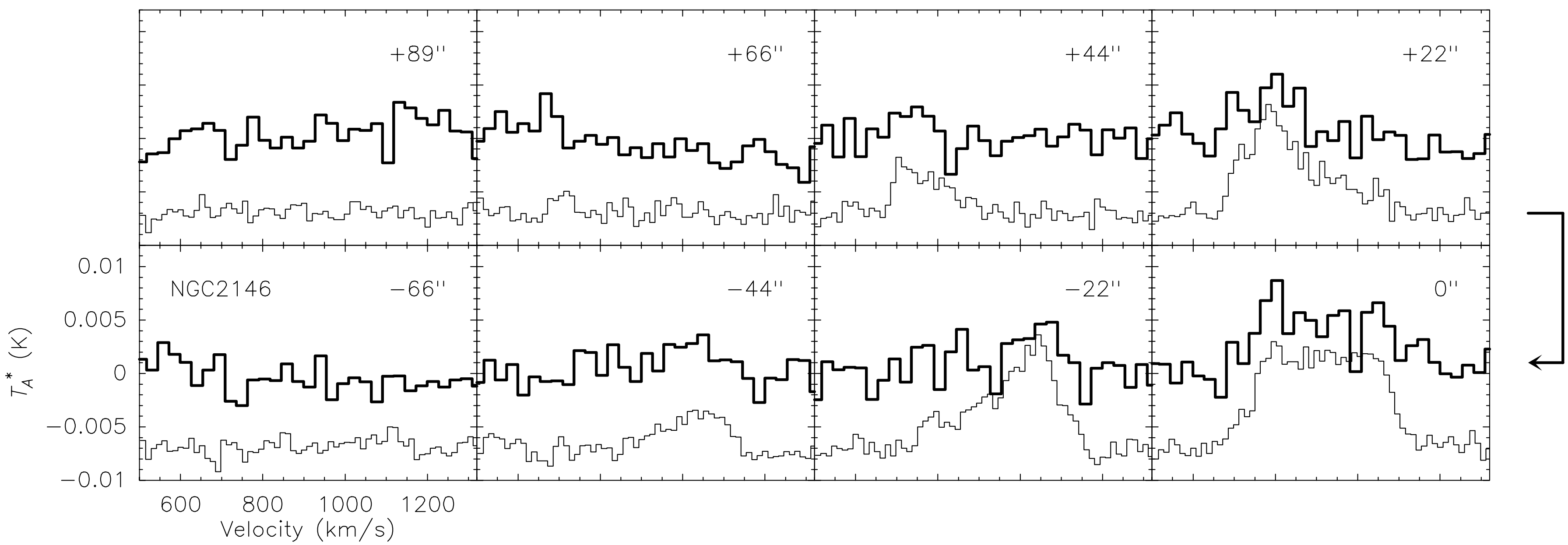

+89''
+66''
+44''
+22''
NGC2146
−66''
−44''
−22''
0''
0.01
0.005
0
−0.005
−0.01
T_A^* (K)
600
800
1000
1200
Velocity (km/s)

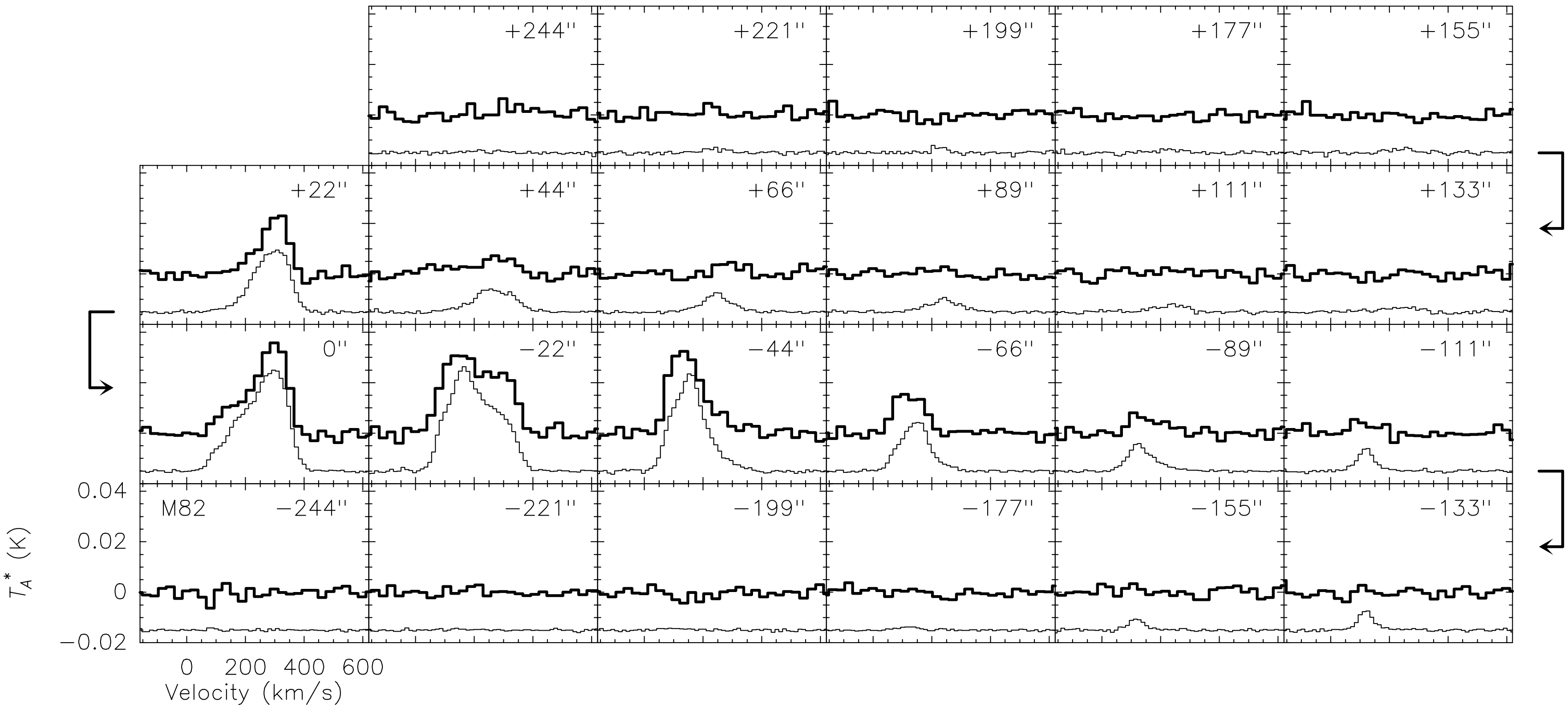
+244''
+221''
+199''
+177''
+155''
+22''
+44''
+66''
+89''
+111''
+133''
0''
−22''
−44''
−66''
−89''
−111''
M82
−244''
−221''
−199''
−177''
−155''
−133''
0.04
0.02
0
−0.02
T_A^* (K)
0 200 400 600
Velocity (km/s)

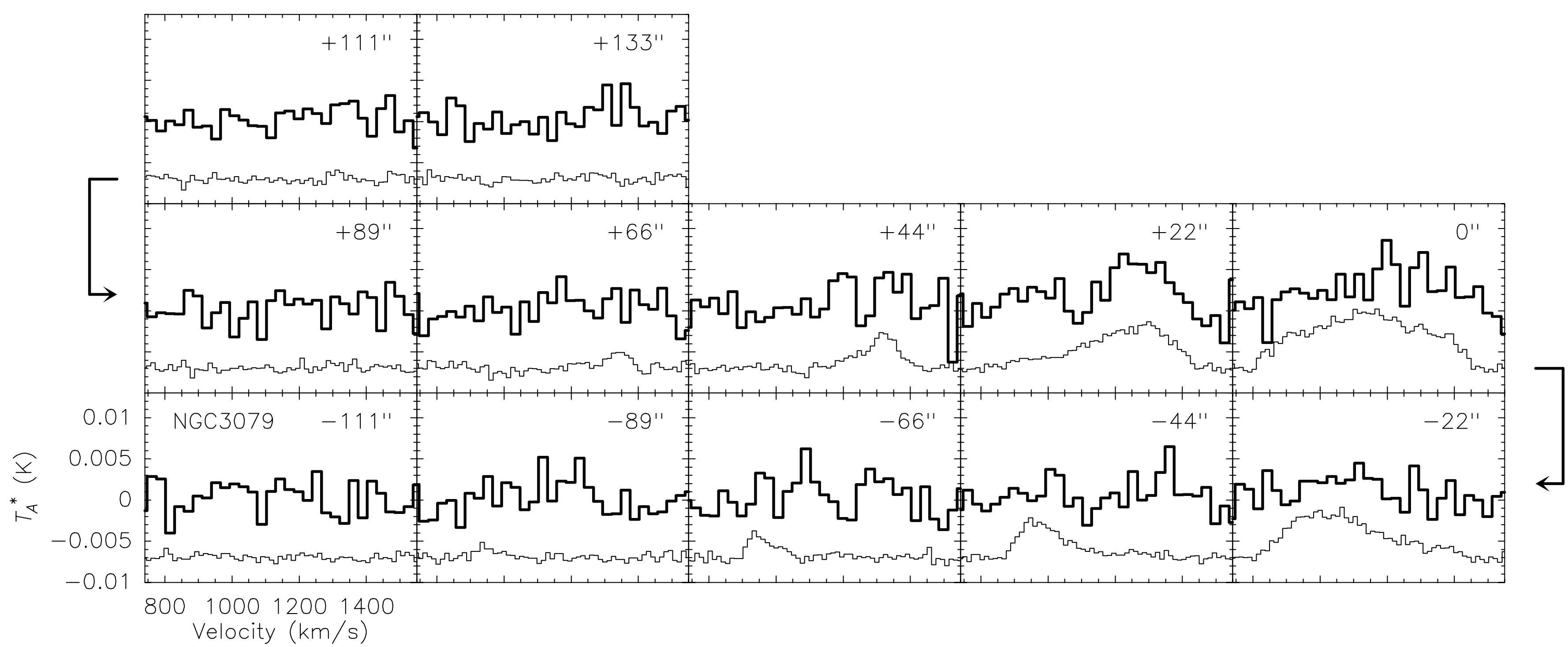

+111''
+133''
+89''
+66''
+44''
+22''
0''
NGC3079
−111''
−89''
−66''
−44''
−22''
0.01
0.005
0
−0.005
−0.01
T_A^* (K)
800
1000
1200
1400
Velocity (km/s)

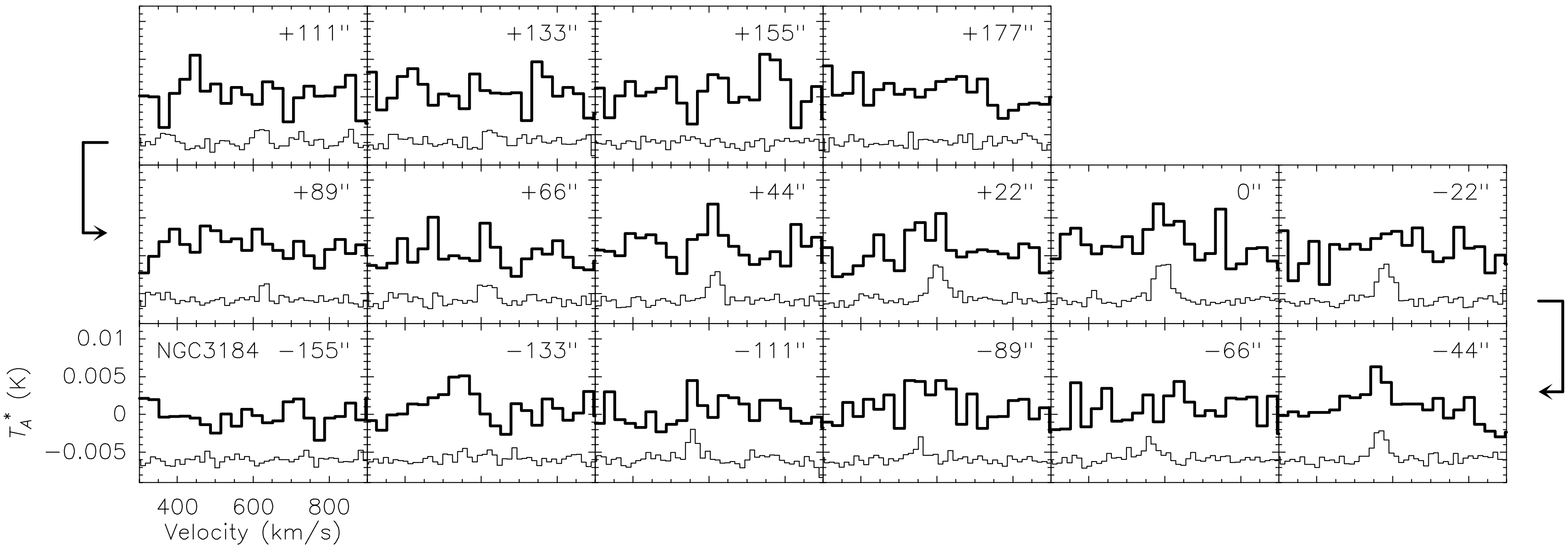

+111''
+133''
+155''
+177''
+89''
+66''
+44''
+22''
0''
−22''
NGC3184 −155''
−133''
−111''
−89''
−66''
−44''
0.01
0.005
0
−0.005
T_A^* (K)
400 600 800
Velocity (km/s)

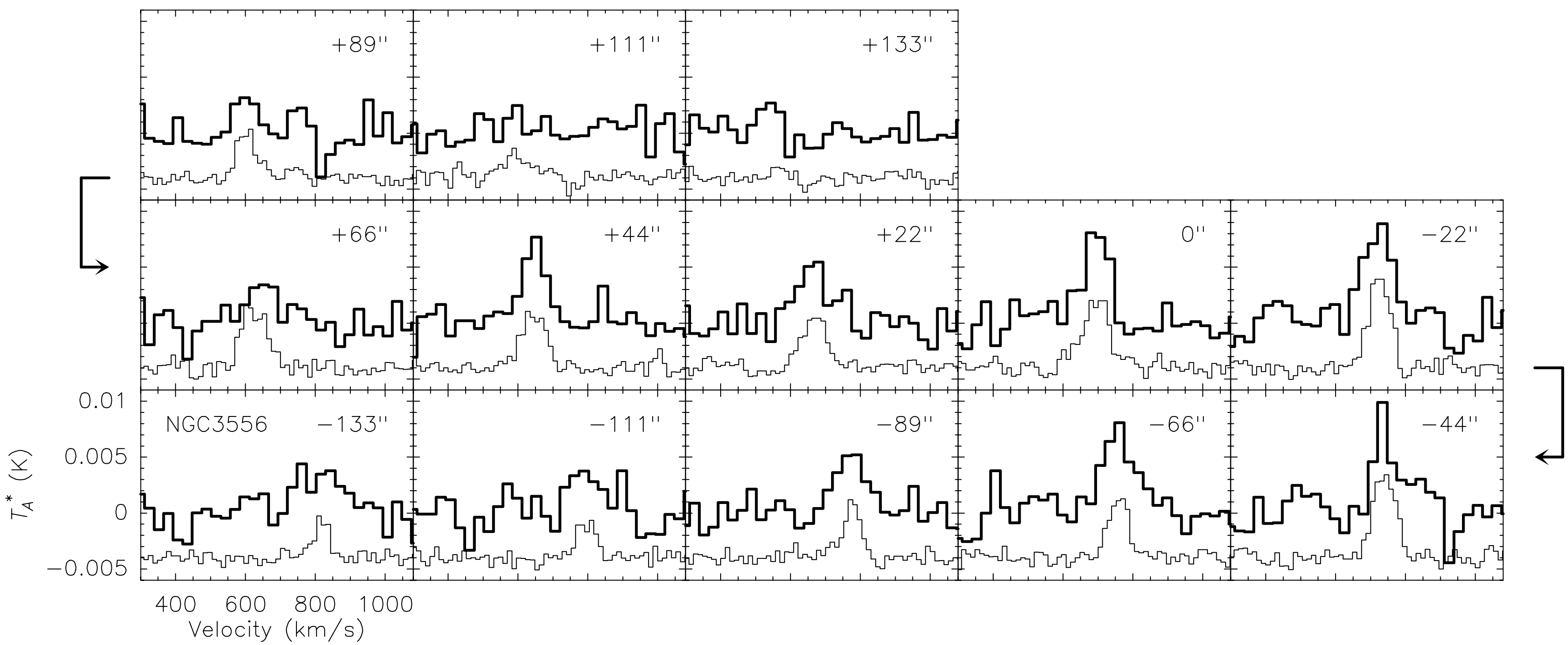

+89''
+111''
+133''
+66''
+44''
+22''
0''
−22''
NGC3556
−133''
−111''
−89''
−66''
−44''
0.01
0.005
0
−0.005
T_A^* (K)
400
600
800
1000
Velocity (km/s)

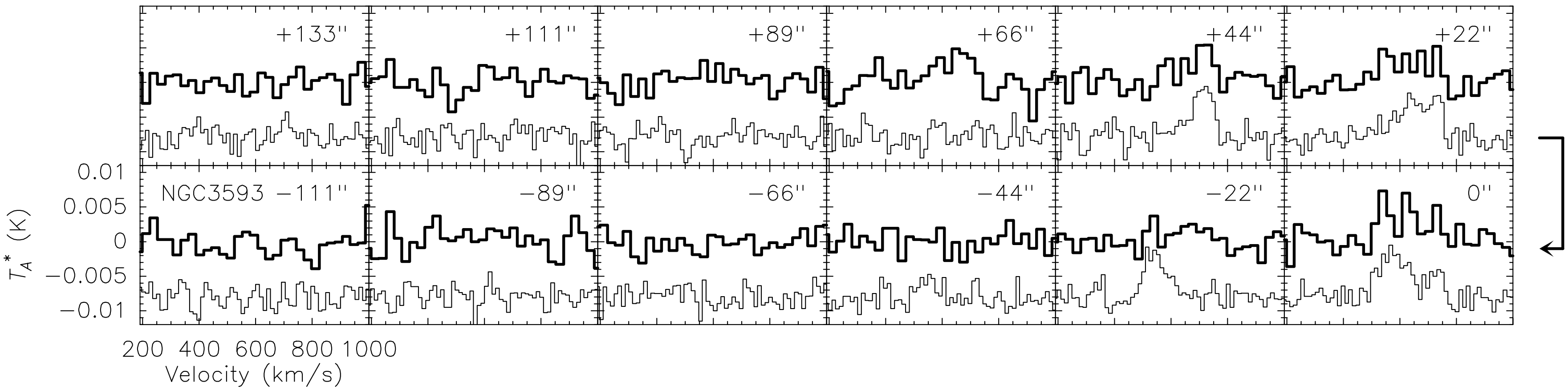
+133''
+111''
+89''
+66''
+44''
+22''
NGC3593 −111''
−89''
−66''
−44''
−22''
0''
0.01
0.005
0
−0.005
−0.01
T_A^* (K)
200 400 600 800 1000
Velocity (km/s)

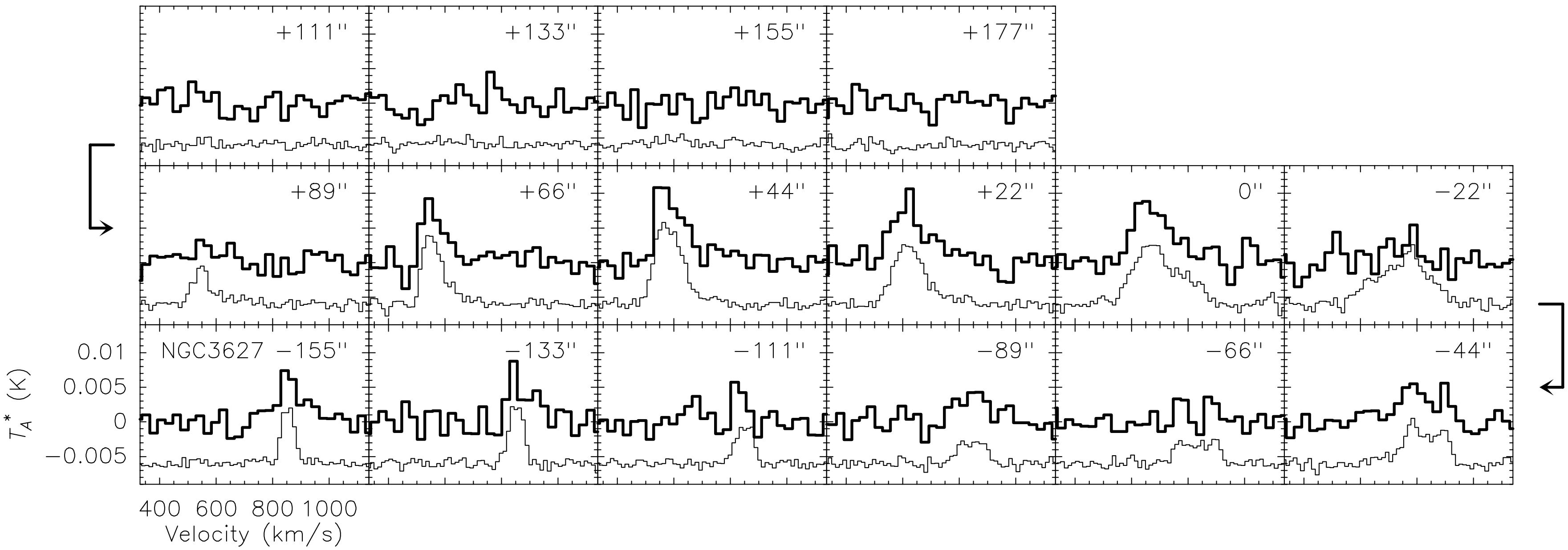

+111''
+133''
+155''
+177''
+89''
+66''
+44''
+22''
0''
−22''
NGC3627 −155''
−133''
−111''
−89''
−66''
−44''
0.01
0.005
0
−0.005
T_A^* (K)
400 600 800 1000
Velocity (km/s)

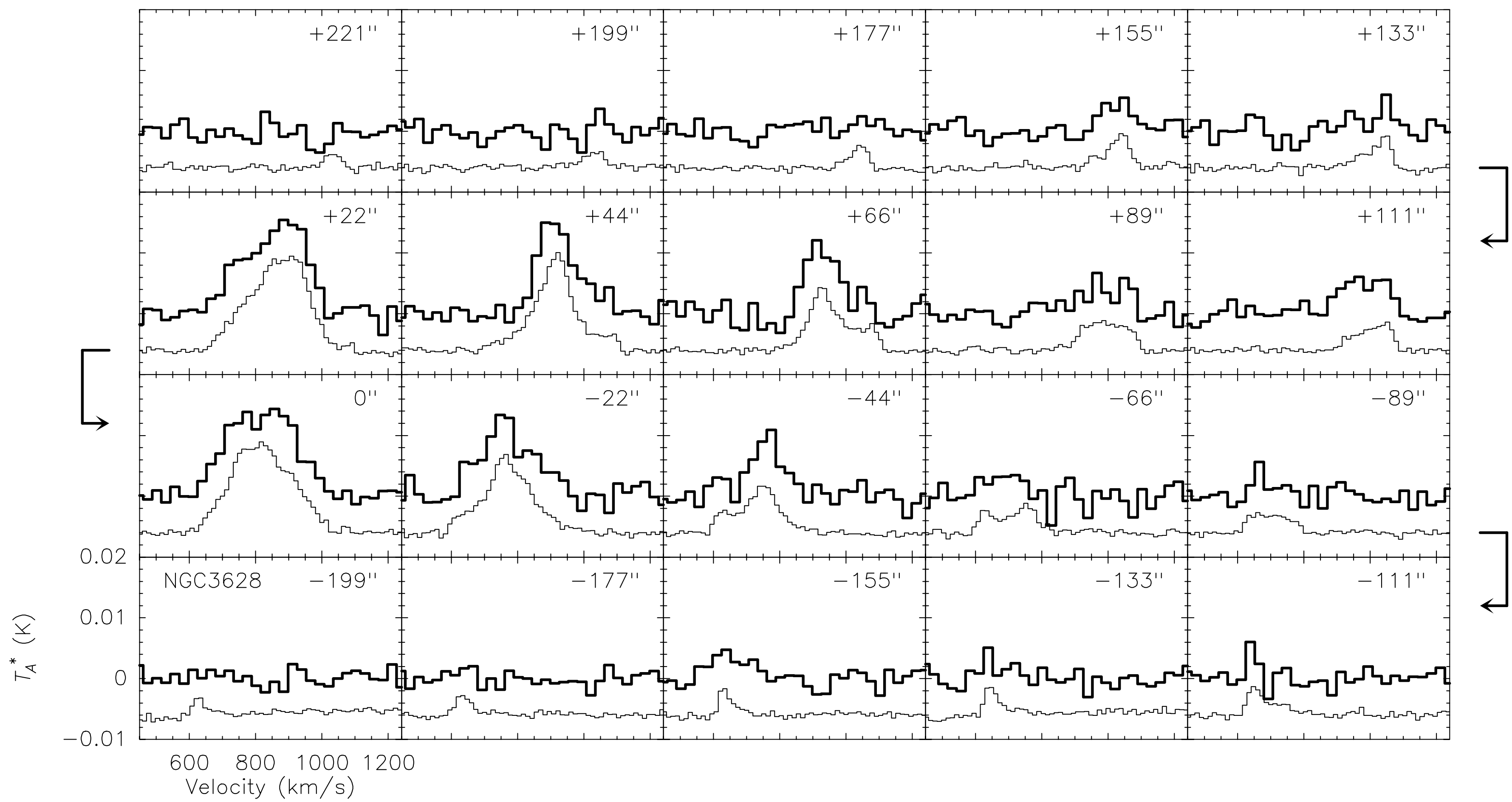

+221''
+199''
+177''
+155''
+133''
+22''
+44''
+66''
+89''
+111''
0''
−22''
−44''
−66''
−89''
NGC3628
−199''
−177''
−155''
−133''
−111''
0.02
0.01
0
−0.01
T_A^* (K)
600 800 1000 1200
Velocity (km/s)

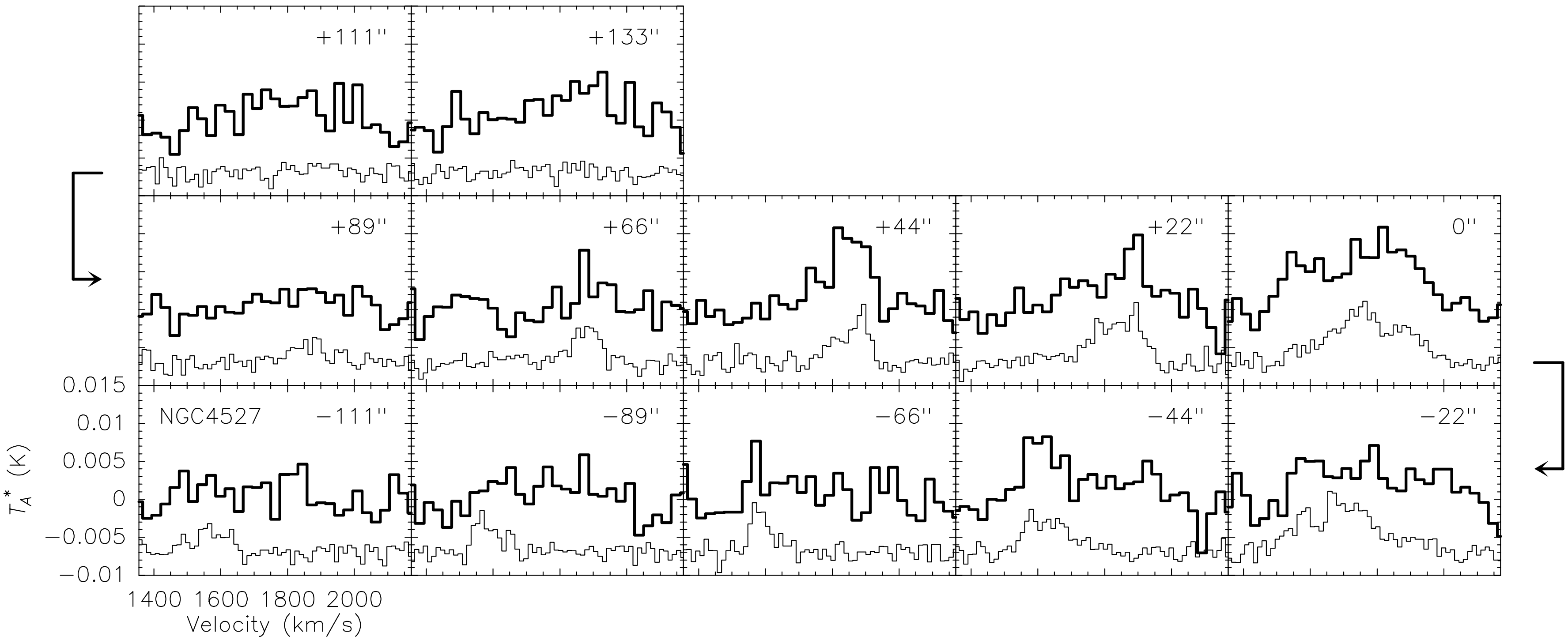

+111''
+133''
+89''
+66''
+44''
+22''
0''
NGC4527
−111''
−89''
−66''
−44''
−22''
0.015
0.01
0.005
0
−0.005
−0.01
T_A^* (K)
1400 1600 1800 2000
Velocity (km/s)

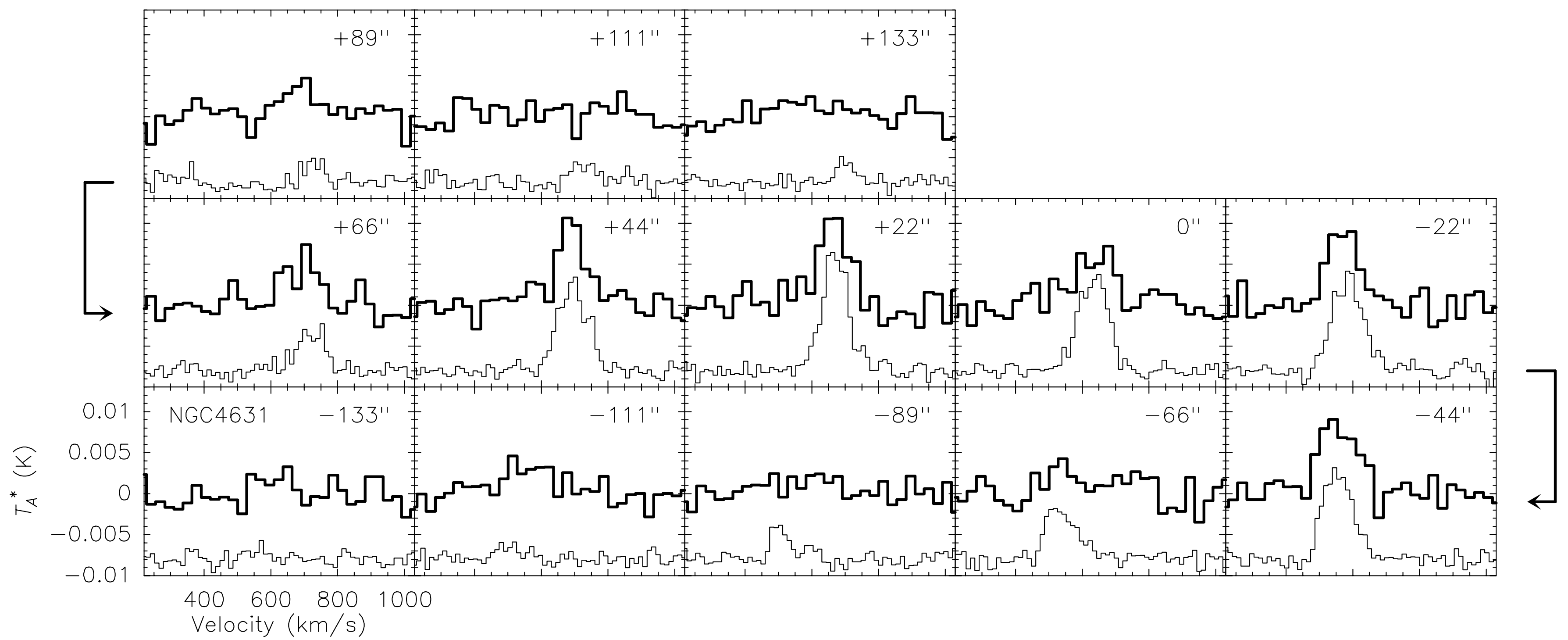
+89''
+111''
+133''
+66''
+44''
+22''
0''
−22''
NGC4631
−133''
−111''
−89''
−66''
−44''
0.01
0.005
0
−0.005
−0.01
T_A^* (K)
400 600 800 1000
Velocity (km/s)

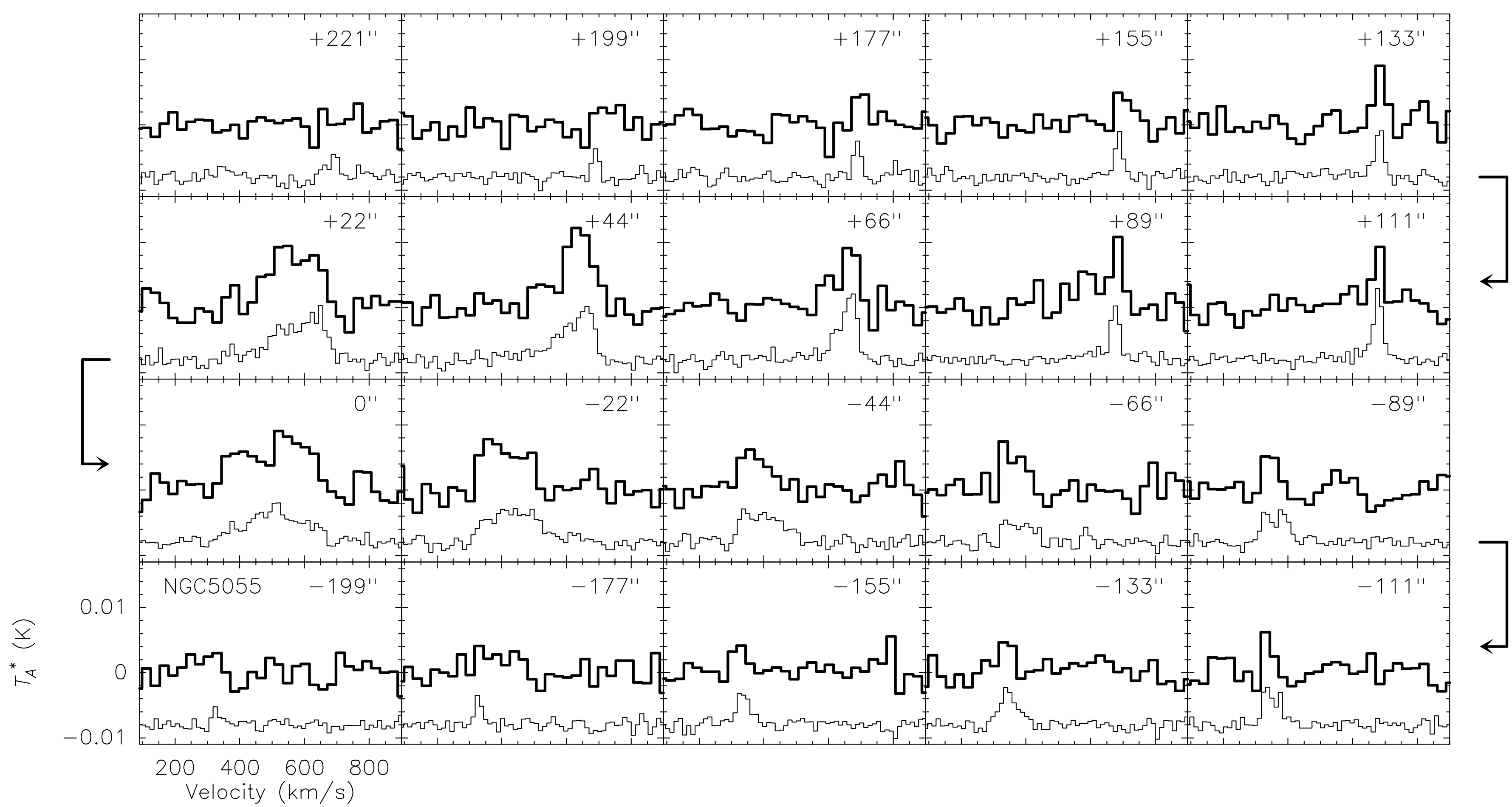

+221''
+199''
+177''
+155''
+133''
+22''
+44''
+66''
+89''
+111''
0''
−22''
−44''
−66''
−89''
NGC5055
−199''
−177''
−155''
−133''
−111''
0.01
0
−0.01
T_A^* (K)
200 400 600 800
Velocity (km/s)

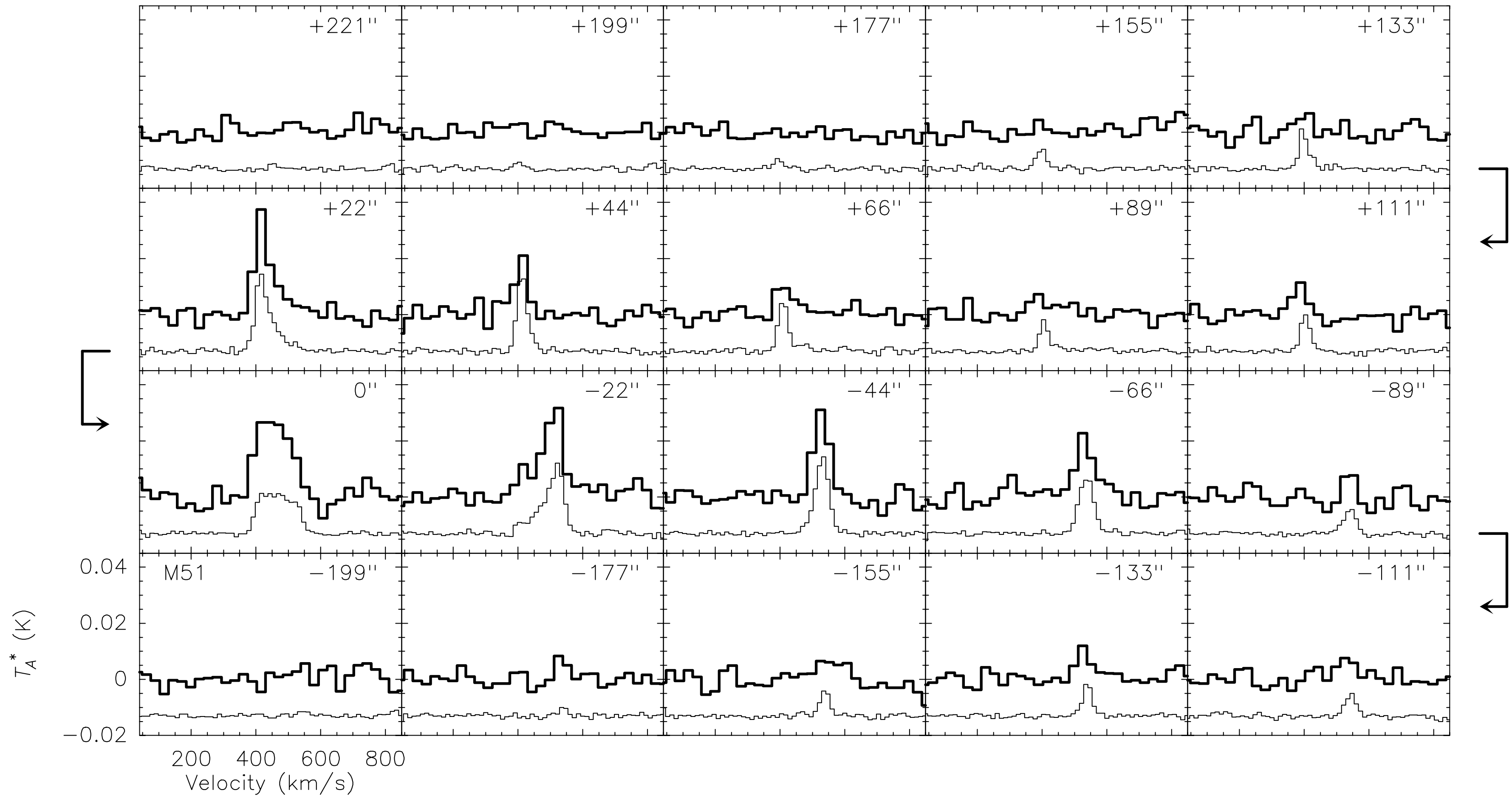

+221''
+199''
+177''
+155''
+133''
+22''
+44''
+66''
+89''
+111''
0''
−22''
−44''
−66''
−89''
M51
−199''
−177''
−155''
−133''
−111''
0.04
0.02
0
−0.02
T_A^* (K)
200
400
600
800
Velocity (km/s)

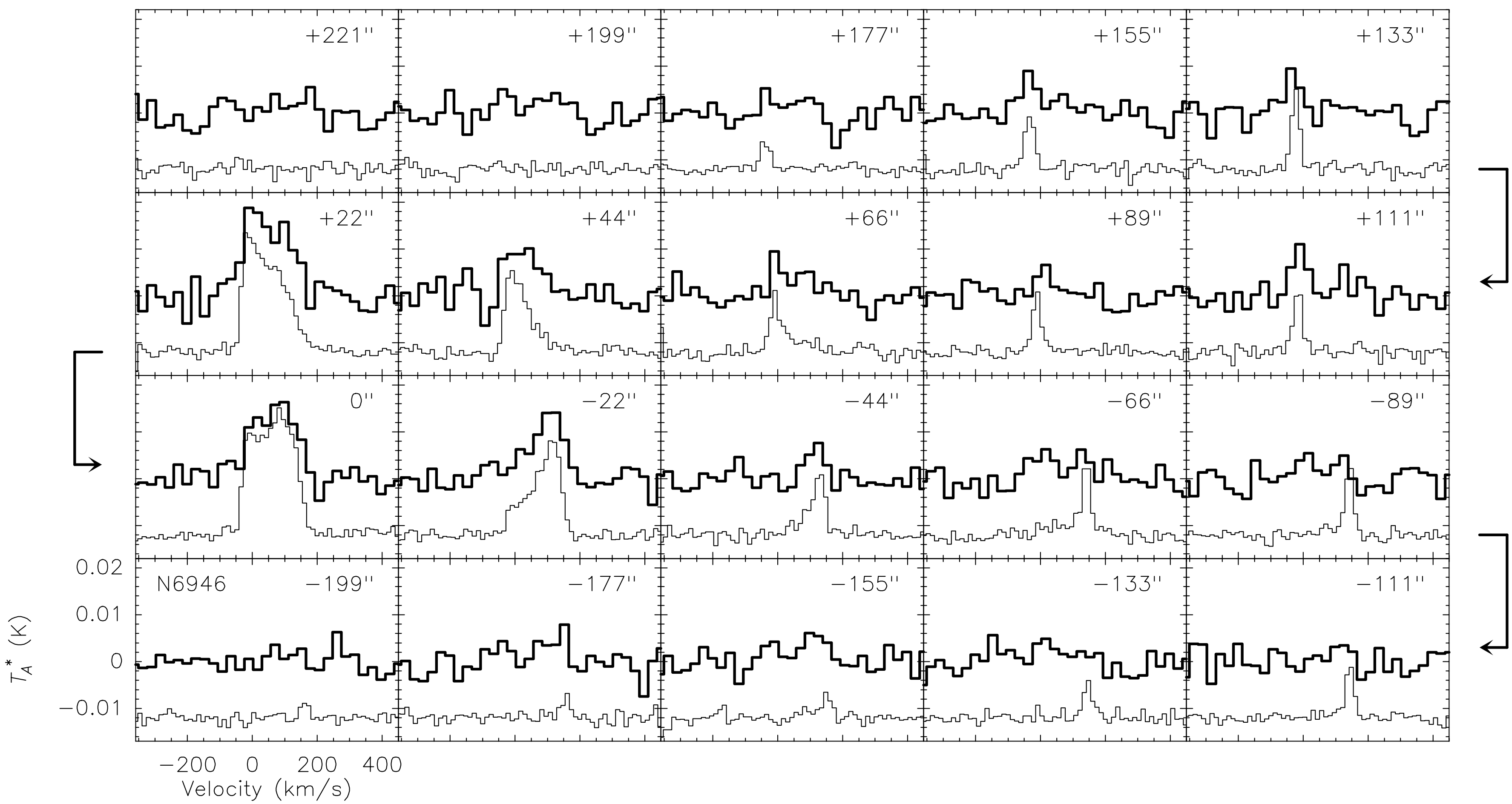
+221''
+199''
+177''
+155''
+133''
+22''
+44''
+66''
+89''
+111''
0''
−22''
−44''
−66''
−89''
N6946
−199''
−177''
−155''
−133''
−111''
0.02
0.01
0
−0.01
T_A^* (K)
−200
0
200
400
Velocity (km/s)

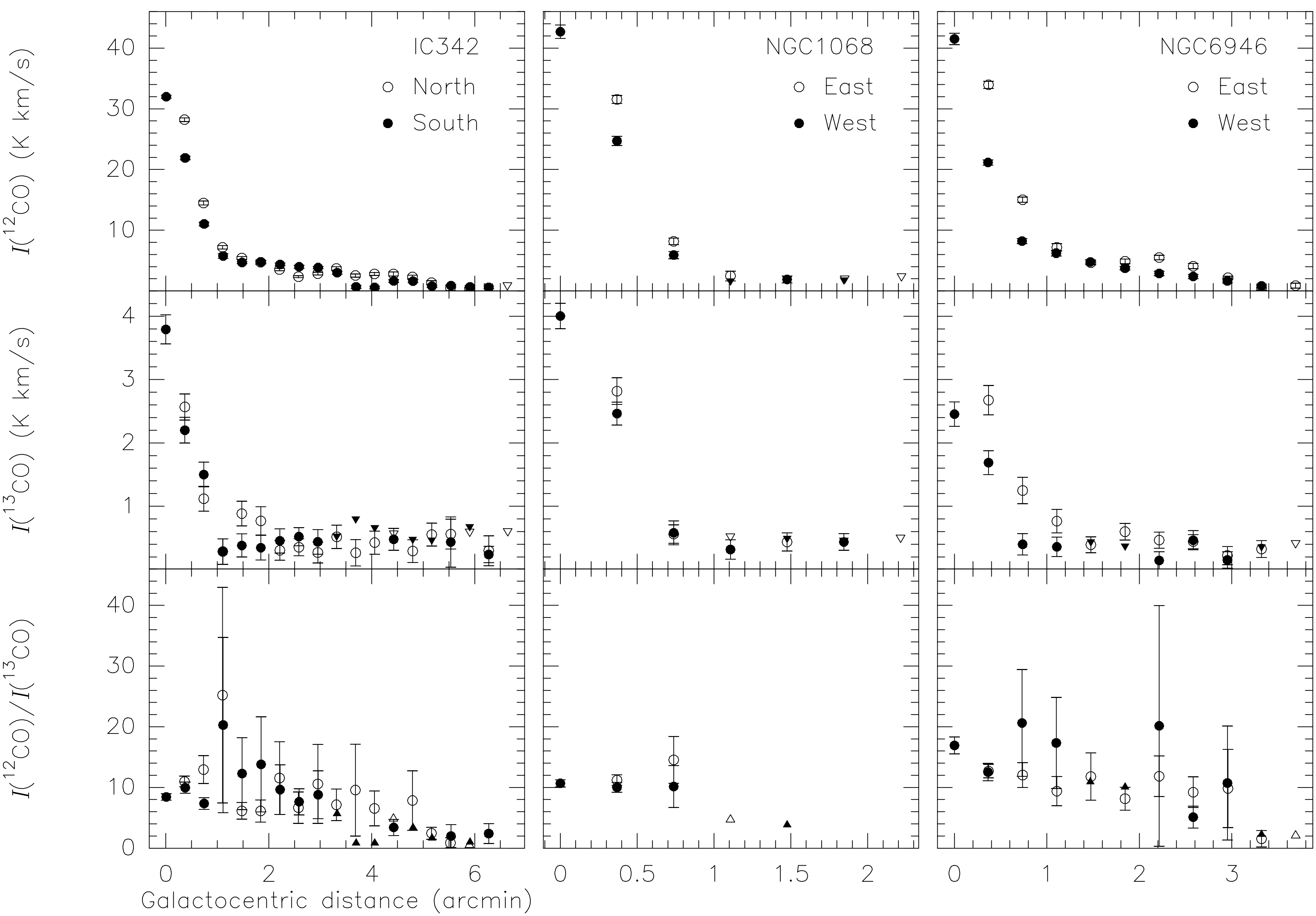
IC342
North
South
NGC1068
East
West
NGC6946
East
West
I(12CO) (K km/s)
I(13CO) (K km/s)
I(12CO)/I(13CO)
Galactocentric distance (arcmin)

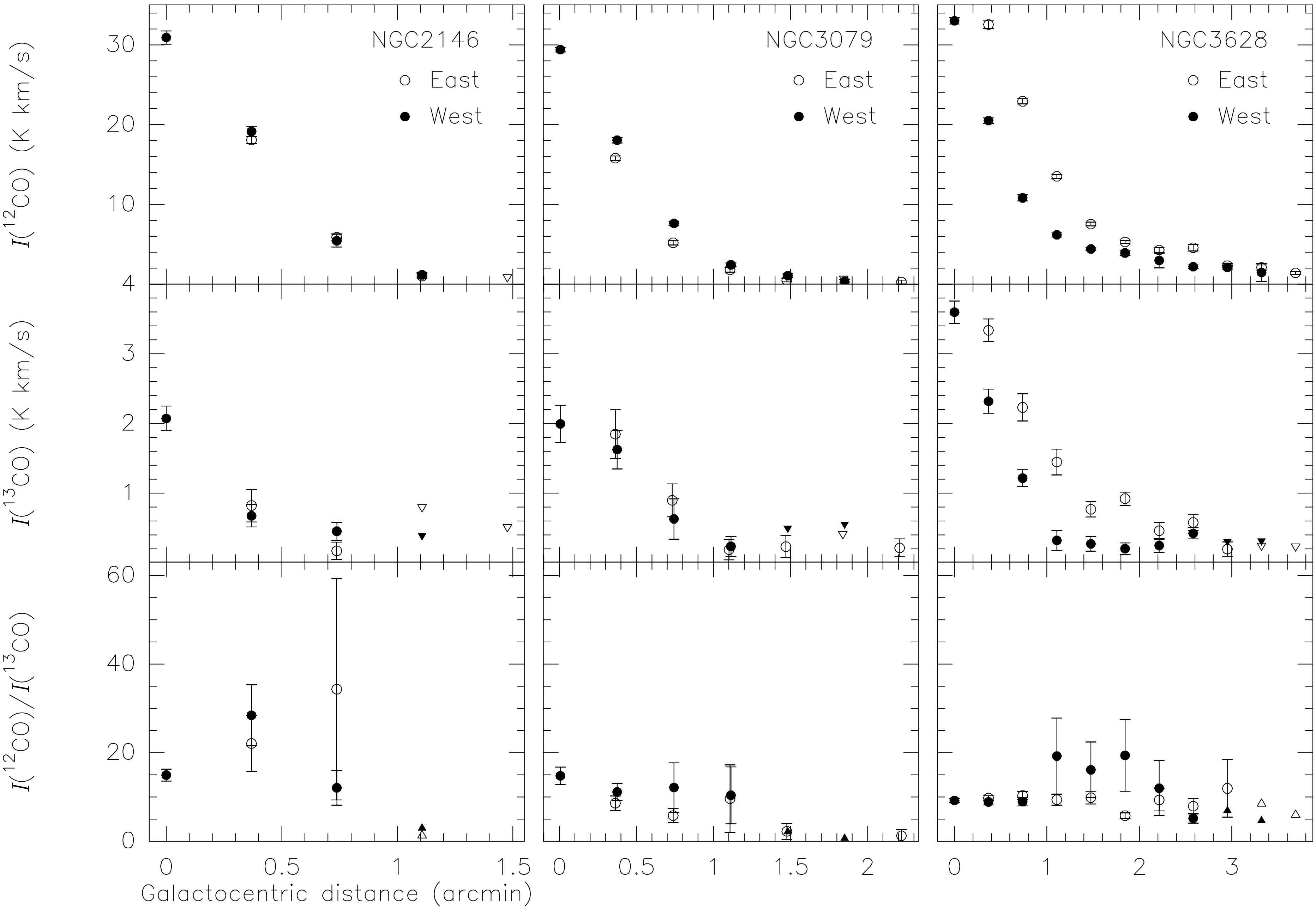
NGC2146
NGC3079
NGC3628
East
West
$I(^{12}CO)$ (K km/s)
$I(^{13}CO)$ (K km/s)
$I(^{12}CO)/I(^{13}CO)$
Galactocentric distance (arcmin)

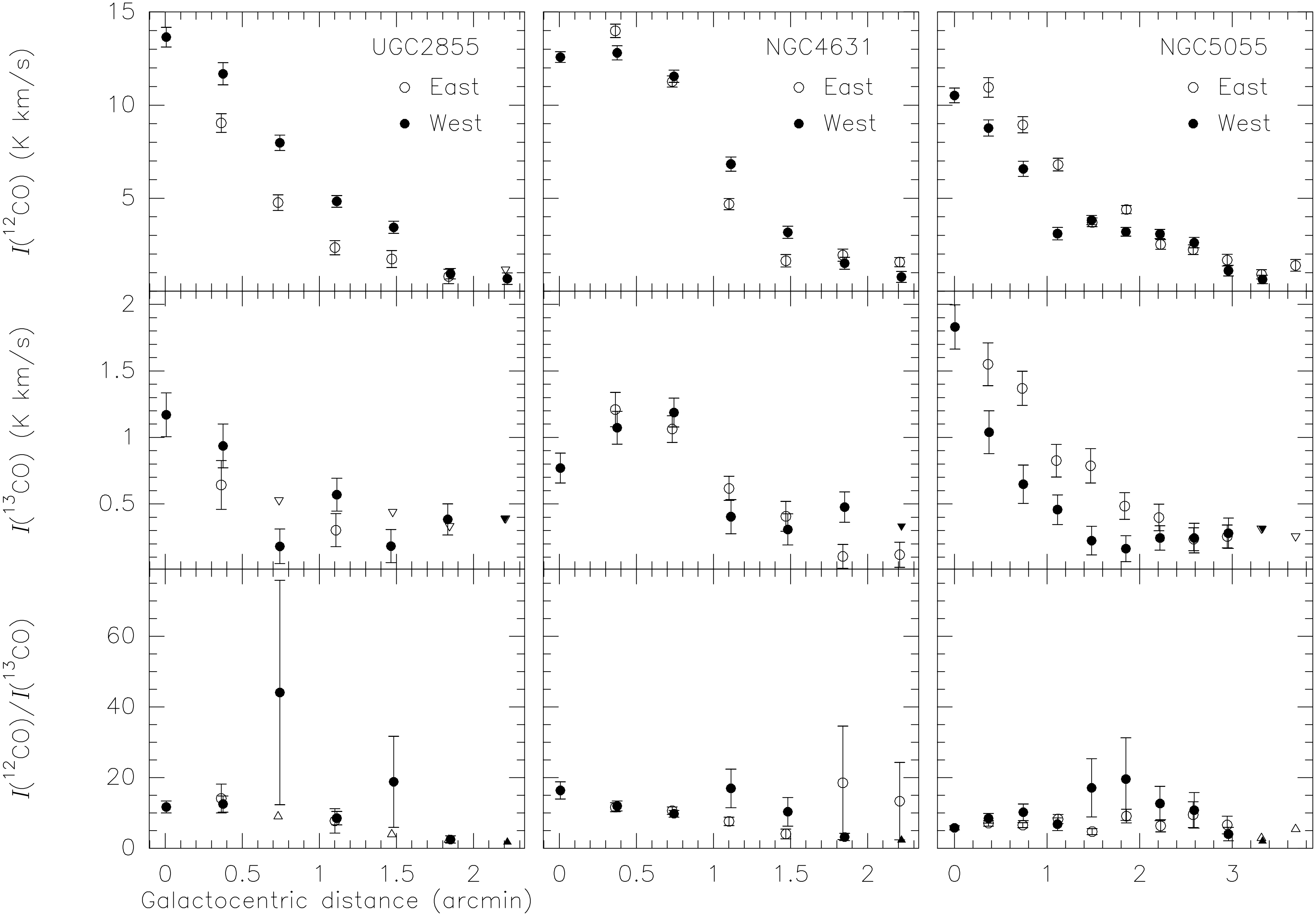

UGC2855
NGC4631
NGC5055
East
West
$I(^{12}CO)$ (K km/s)
$I(^{13}CO)$ (K km/s)
$I(^{12}CO)/I(^{13}CO)$
Galactocentric distance (arcmin)

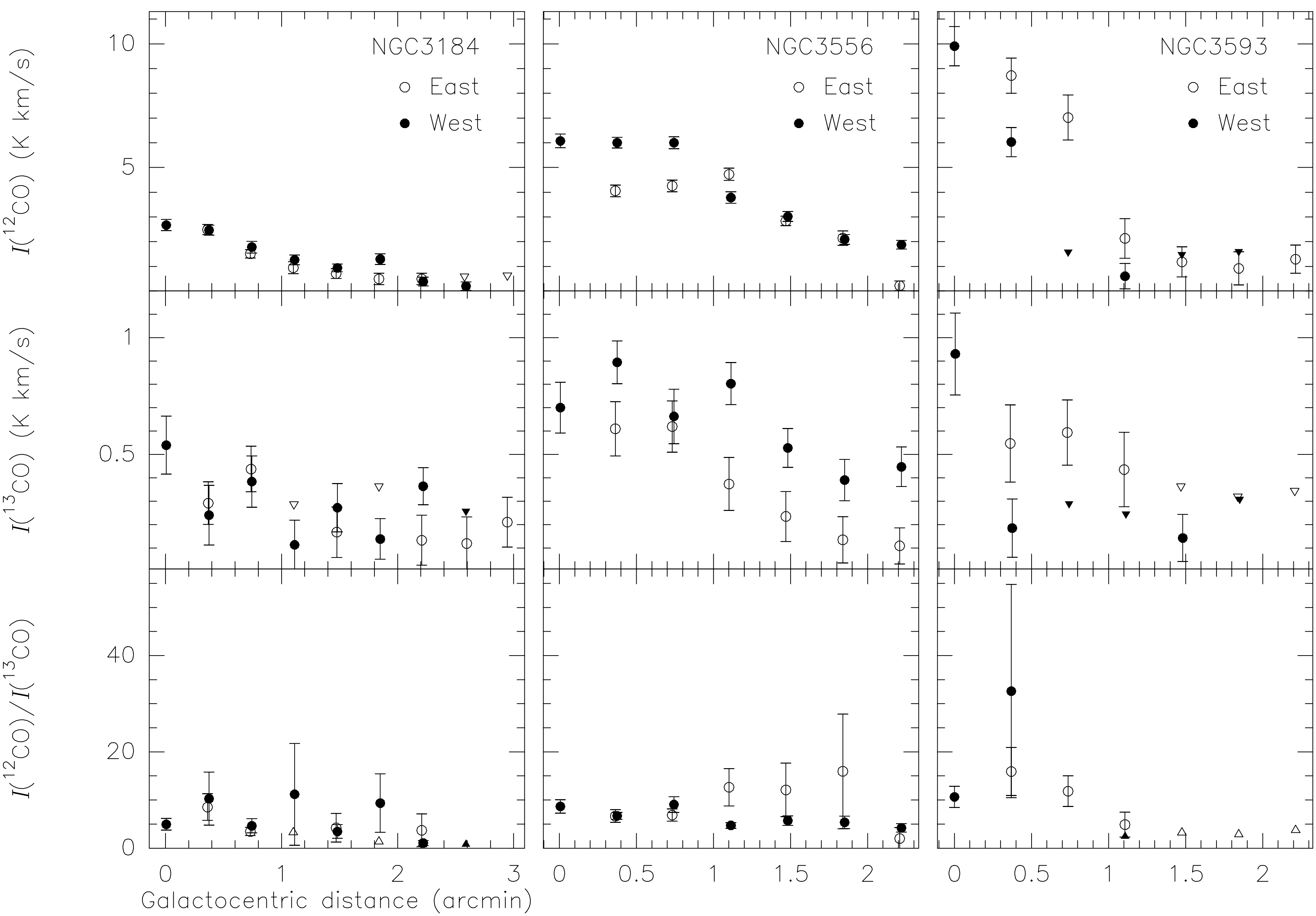
NGC3184
East
West
NGC3556
East
West
NGC3593
East
West
$I(^{12}CO)$ (K km/s)
$I(^{13}CO)$ (K km/s)
$I(^{12}CO)/I(^{13}CO)$
Galactocentric distance (arcmin)

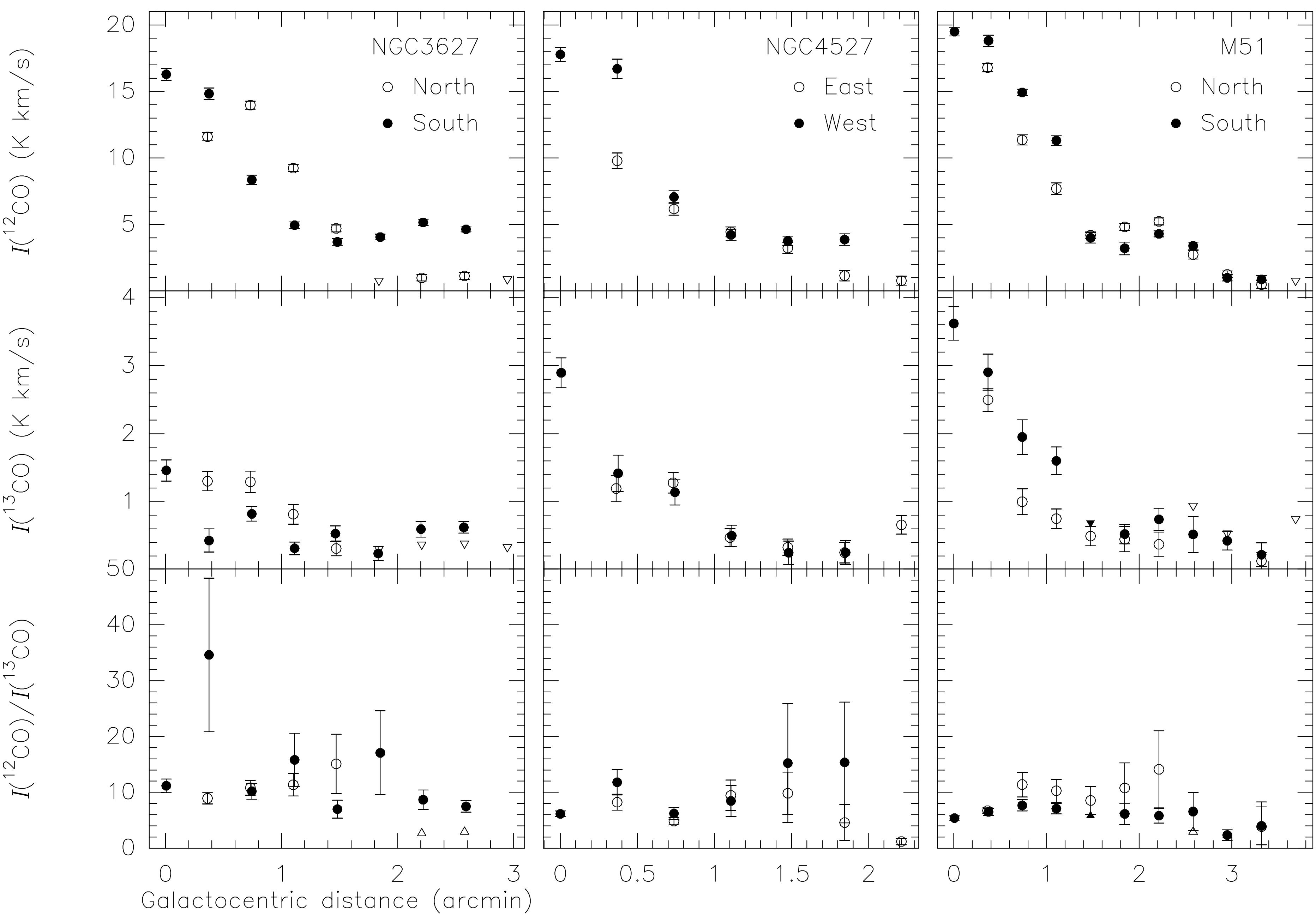
NGC3627
North
South
NGC4527
East
West
M51
North
South
$I(^{12}CO)$ (K km/s)
$I(^{13}CO)$ (K km/s)
$I(^{12}CO)/I(^{13}CO)$
Galactocentric distance (arcmin)

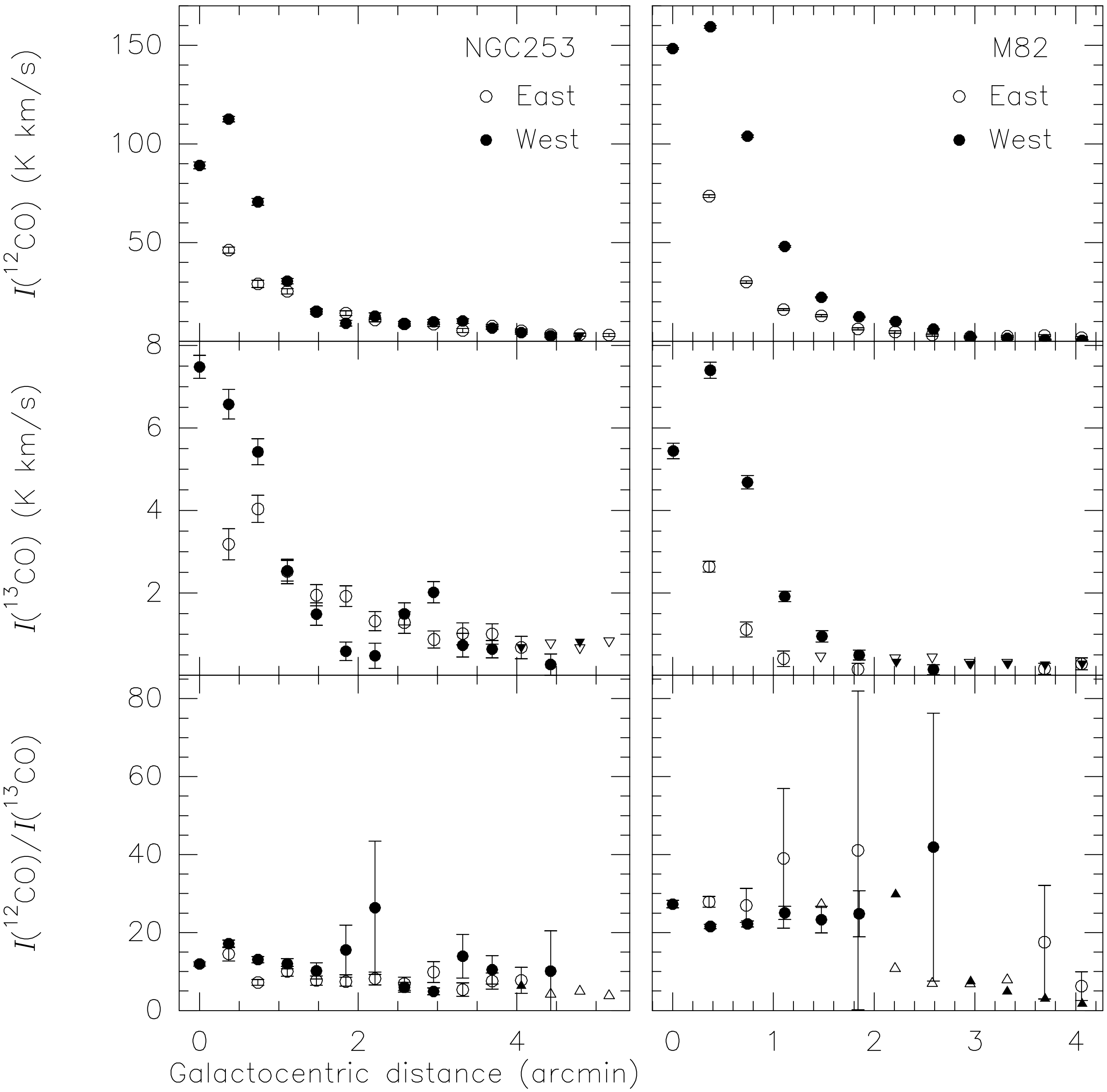

NGC253
East
West
M82
East
West
$I(^{12}CO)$ (K km/s)
$I(^{13}CO)$ (K km/s)
$I(^{12}CO)/I(^{13}CO)$
Galactocentric distance (arcmin)

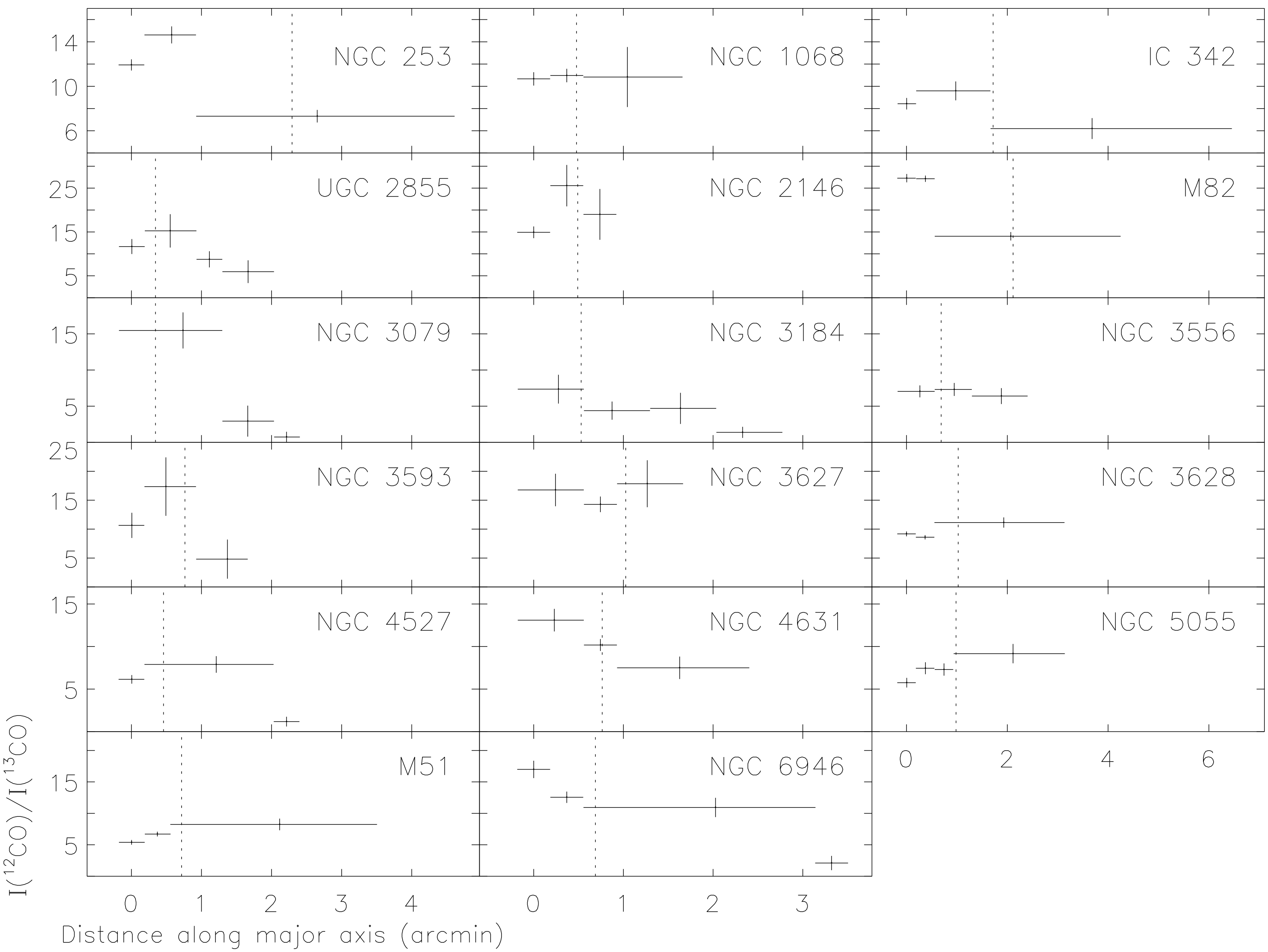
NGC 253
NGC 1068
IC 342
UGC 2855
NGC 2146
M82
NGC 3079
NGC 3184
NGC 3556
NGC 3593
NGC 3627
NGC 3628
NGC 4527
NGC 4631
NGC 5055
M51
NGC 6946
I(¹²CO)/I(¹³CO)
Distance along major axis (arcmin)

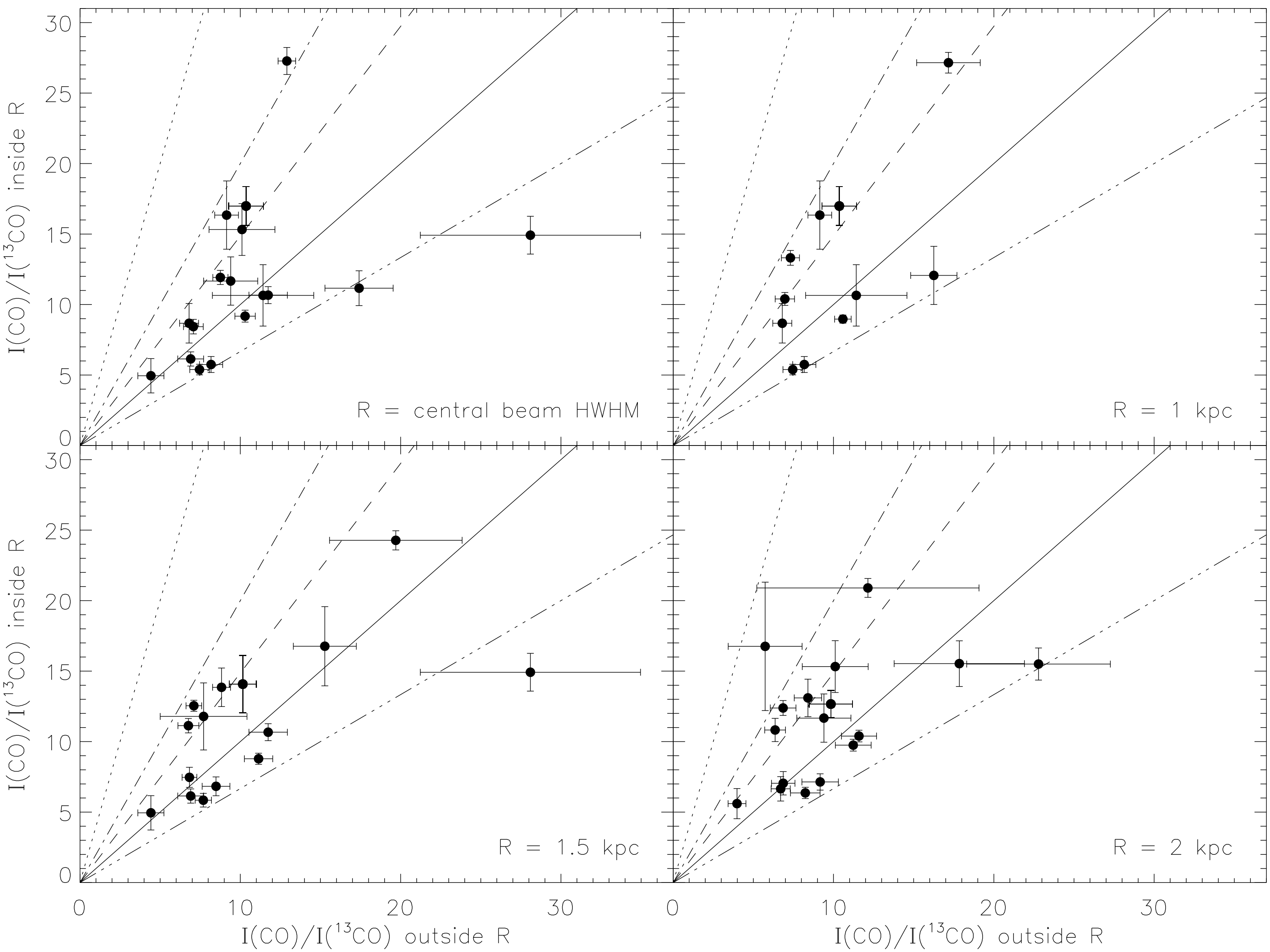
I(CO)/I(^{13}CO) inside R
I(CO)/I(^{13}CO) outside R
R = central beam HWHM
R = 1 kpc
R = 1.5 kpc
R = 2 kpc

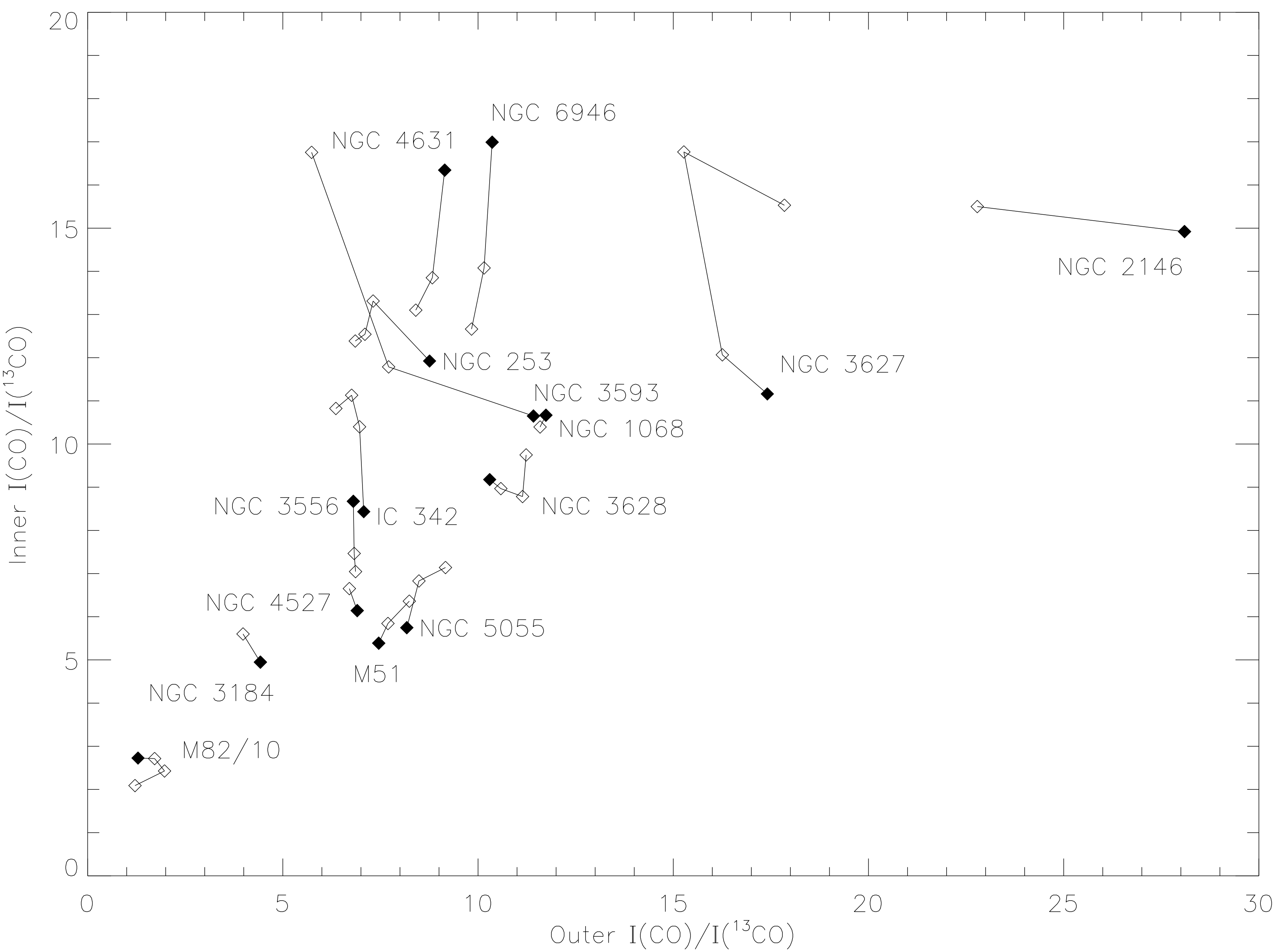
NGC 6946
NGC 4631
NGC 2146
NGC 253
NGC 3627
NGC 3593
NGC 1068
NGC 3556
IC 342
NGC 3628
NGC 4527
NGC 5055
M51
NGC 3184
M82/10
Inner I(CO)/I(13CO)
Outer I(CO)/I(13CO)
0
5
10
15
20
25
30

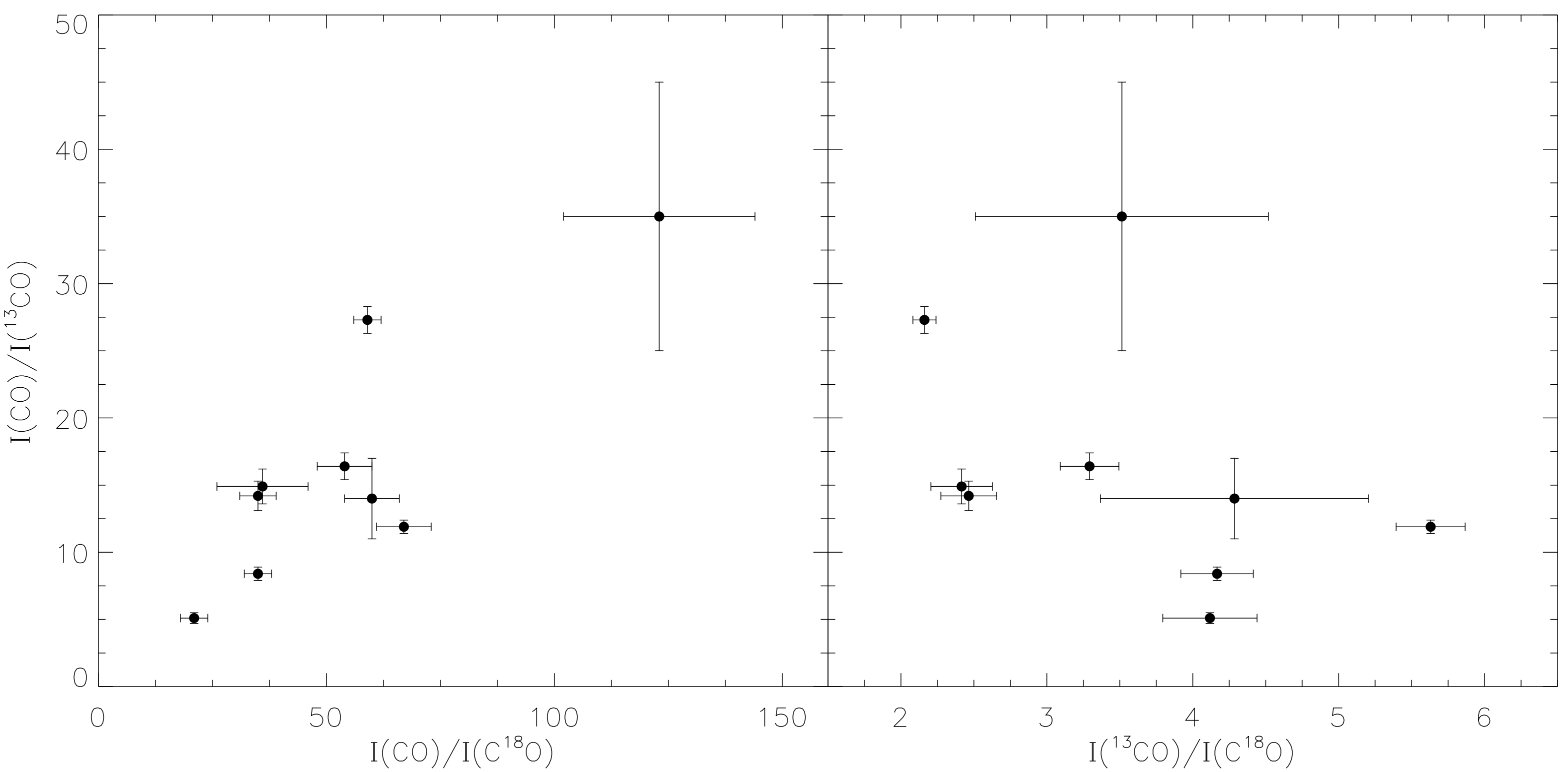

I(CO)/I(^{13}CO)
0
10
20
30
40
50
0
50
100
150
I(CO)/I(C^{18}O)
2
3
4
5
6
I(^{13}CO)/I(C^{18}O)

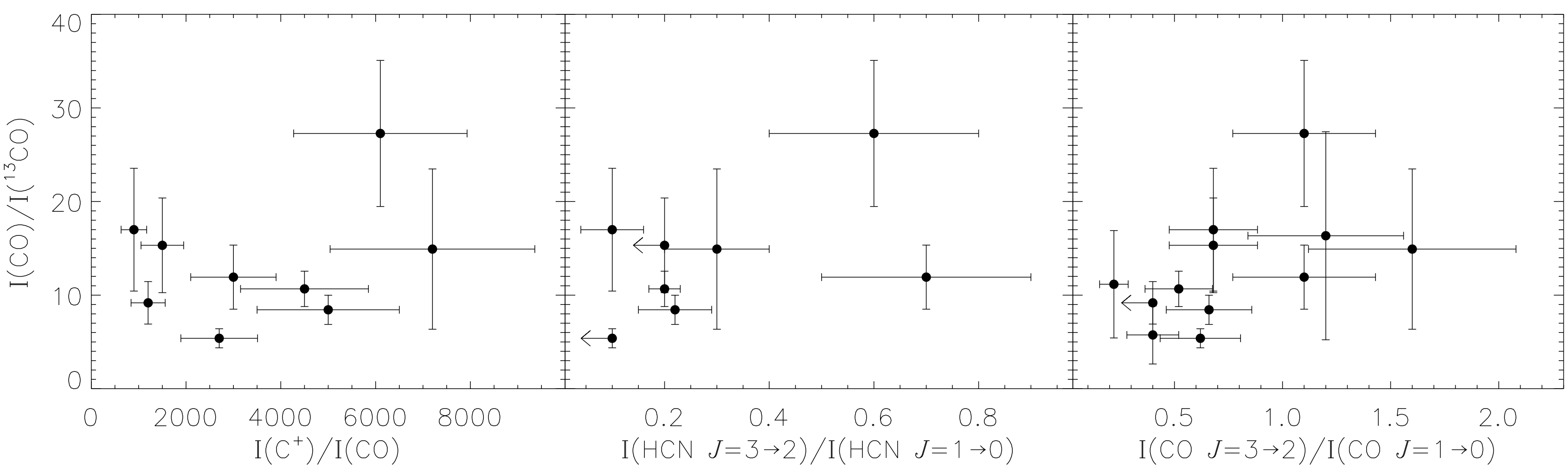
I(CO)/I(^{13}CO)
I(C$^+$)/I(CO)
I(HCN J=3→2)/I(HCN J=1→0)
I(CO J=3→2)/I(CO J=1→0)

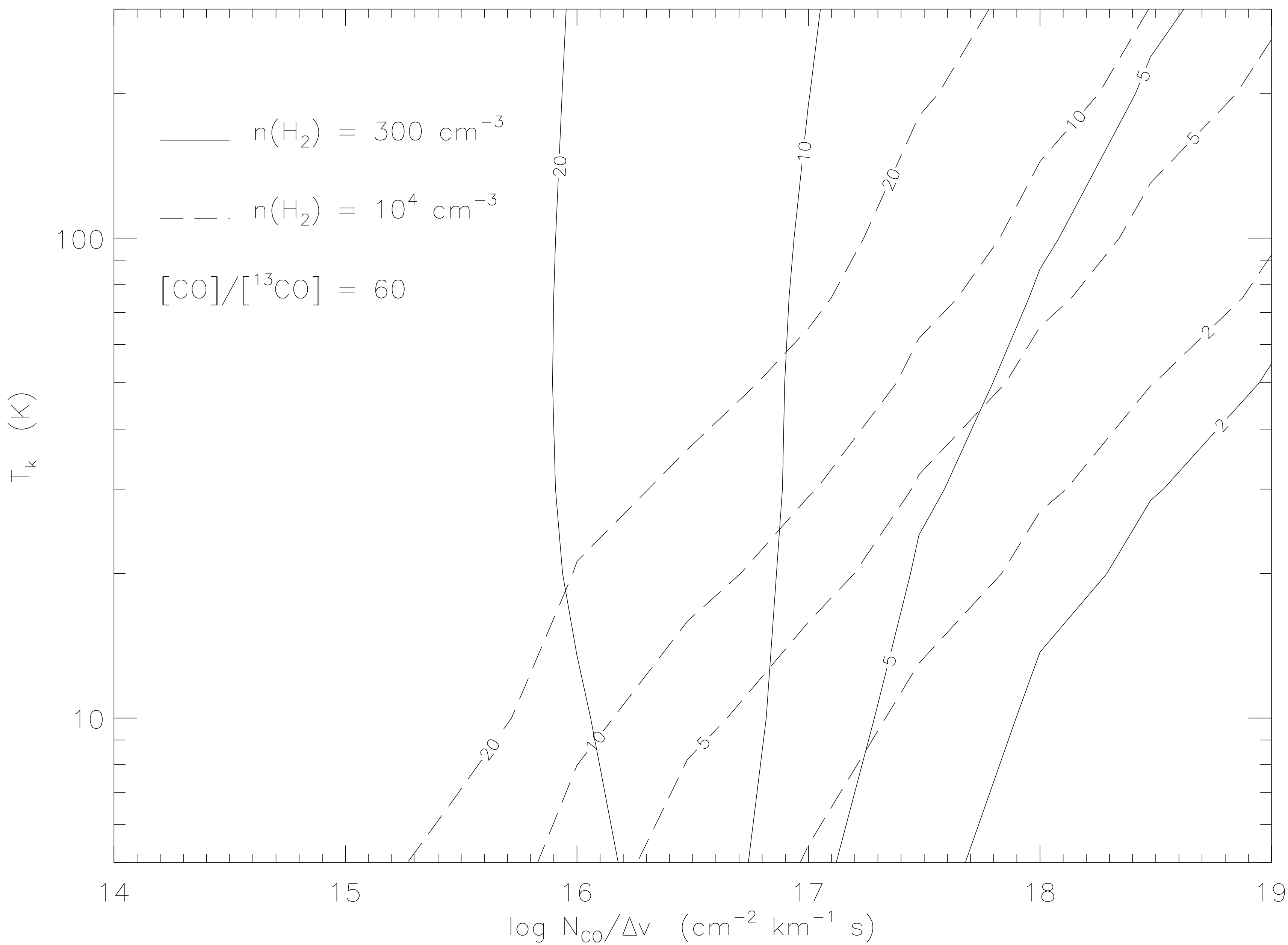

n(H2) = 300 cm^-3
n(H2) = 10^4 cm^-3
[CO]/[13CO] = 60
20
10
5
2
100
10
14
15
16
17
18
19
T_k (K)
log N_CO/Δv (cm^-2 km^-1 s)